energies

MDPI

Article

Dandelion Optimizer-Based Combined Automatic Voltage Regulation and Load Frequency Control in a Multi-Area, Multi-Source Interconnected Power System with Nonlinearities

Tayyab Ali [1], Suheel Abdullah Malik [1], Amil Daraz [2], Sheraz Aslam [3,*] and Tamim Alkhalifah [4,*]

[1] Department of Electrical and Computer Engineering, Faculty of Engineering and Technology, International Islamic University, Islamabad 44000, Pakistan
[2] School of Information science and Engineering, Ningbotech University, Ningbo 315100, China
[3] Department of Electrical Engineering, Computer Engineering and Informatics, Cyprus University of Technology, 3036 Limassol, Cyprus
[4] Department of Computer, College of Science and Arts in ArRass, Qassim University, Ar Rass 52571, Saudi Arabia
* Correspondence: sheraz.aslam@cut.ac.cy (S.A.); tkhliefh@qu.edu.sa (T.A.)

Abstract: Frequency, voltage, and power flow between different control zones in an interconnected power system are used to determine the standard quality of power. Therefore, the voltage and frequency control in an IPS is of vital importance to maintaining real and reactive power balance under varying load conditions. In this paper, a dandelion optimizer (DO)-based proportional-integral-proportional-derivative (PI-PD) controller is investigated for a realistic multi-area, multi-source, realistic IPS with nonlinearities. The output responses of the DO-based PI-PD were compared with the hybrid approach using artificial electric field-based fuzzy PID algorithm (HAEFA), Archimedes optimization algorithm (AOA)-based PI-PD, learning performance-based behavior optimization (LPBO)-based PI-PD and modified particle swarm optimization (MPSO)-based PI-PD control schemes in a two-area network with 10% step load perturbation (SLP). The proposed strategy was also investigated in a two- and three-area IPS in the presence of different nonlinearities and SLPs. The simulation results and the comprehensive comparison between the different control schemes clearly confirm that the proposed DO-based PI-PD is very effective for realistic, multi-area multi-source IPS with nonlinearities.

Keywords: automatic voltage regulator; dandelion optimizer; load frequency control multi-area; multi-source interconnected power system; nature-inspired optimization; nonlinear power system and PI-PD controller

Citation: Ali, T.; Malik, S.A.; Daraz, A.; Aslam, S.; Alkhalifah, T. Dandelion Optimizer-Based Combined Automatic Voltage Regulation and Load Frequency Control in a Multi-Area, Multi-Source Interconnected Power System with Nonlinearities. *Energies* **2022**, *15*, 8499. https://doi.org/10.3390/en15228499

Academic Editor: Abu-Siada Ahmed

Received: 13 October 2022
Accepted: 8 November 2022
Published: 14 November 2022

1. Introduction

It is vital in a power system to maintain electrical power at the desired voltage and frequency. The load is always dynamic and varies over time. The difference between generation and load demand creates an imbalance between reactive and active power in the system [1]. This imbalance causes fluctuations in the voltage, frequency and tie-line power. Active power affects the frequency of the system, while reactive power depends on the system voltage. In order to maintain the desired and reliable voltage with frequency in a power system, two loops are built into the power system: a load frequency control (LFC) and an automatic voltage regulator (AVR). The AVR loop essentially reduces voltage fluctuations to meet reactive power requirements from a generator excitation mechanism, while the LFC loop reduces frequency fluctuations by modifying the active power magnitude through its governor action. Voltage and frequency controllers have gained importance with the growth in interconnected systems and have made the operation of power systems more reliable. The design of a proper control strategy is important to minimizing frequency and terminal voltage deviations as well as minimizing the variations of power flow in

the tie-line [2]. Moreover, the performance of a controller solely depends upon the tuning methodology. Therefore, the control design and tuning scheme both are very important for the optimal control of an IPS. In order to acquire adequate and stable power, an effort has been made in this research to simultaneously control LFC and AVR loops using a nature-inspired, computation-based control methodology. The classical PID controller and its variants are widely used for the individual and combined control of AVR-LFC control loops due to their simpler implementation and design. For example, a HAEFA-based fuzzy PID controller was explored in a two-area multi-source IPS in the presence of different energy storage technologies, such as UCs, SMES and RFBs [3]. In ref. [4], the authors presented a PI-PD controller based on recently introduced, nature-inspired meta-heuristics including AOA, LPBO and MPSO for a multi-area IPS. A DPO-based PIDA controller was explored for a two-area multi-source IPS with two solar energy and three bioenergy sources [5]. In ref. [6], an AFA-based CPDN-FOPIDN controller was employed in a three-area IPS with nonlinearities such as GDB and GRC. Further, an HVDC link and different energy storage devices were also incorporated to improve the performance of the system. A CFOTDN-FOPDN controller designed with AFA was proposed for a two-area multi-source, nonlinear IPS [7]. An AFA-based CFPD-TID controller was suggested for a three-area IPS in the presence of GDB, GRC, RFBs and HVDC link [8]. The authors also recommended an HHO-based 2DOF-ITDF controller for a three-area multi-source, nonlinear IPS with reheat thermal, wind, solar thermal and dish-Stirling generation units [9]. In [10], the authors examined an ADRC controller based on second-order-error-driven control law in an IPS. The generation units in the IPS included solar, geothermal, wind and EVs. The HHO-tuned TIDF controller was also investigated for a three-area multi-sources nonlinear IPS [11]. APIDA controller tuned with hFPAPFA was also applied to a single-area, single-source IPS [12]. An FA-based PID controller was explored for a two-area multi-source IPS with nonlinearities such as TD, GRC and GDB [13]. In ref. [14], the authors presented a PIDD controller for a two-area, nonlinear IPS incorporating UPFC and SMES. A GWO was utilized for the tuning of a PIDD controller. The NLTA-based PID controller design was also proposed for a two-area, linear IPS [15]. For a two-area IPS with reheat and non-reheat thermal power plants as generating units, SCA-based PIDA and PI controllers were explored for LFC and AVR loops, respectively [16]. In the presence of GRC, a DE-AEFA-based PID was evaluated for a two-area IPS. An HVDC link, IPFC and RFBs were also incorporated in the power system for satisfactory improvements [17,18]. In ref. [19], the authors suggested an IPSO-based CPSS controller for a single-area, nonlinear IPS. An FA-based PID controller was investigated for a two-area multi-source IPS with non-reheat thermal- and hydro-generating units [20]. A FOPID controller was explored for a two-area, nonlinear IPS. The optimum parameters of FOPID were found using MSO [21]. The response of a two-area multi-source, nonlinear IPS incorporating IPFC, SMES, GDB and GRC was investigated with LSA-based PIDF/PID^{u}F controllers [22]. ZN-based PID and FLC controllers were applied to a single-area, single-source IPS [23]. In ref. [24], the authors examined a single-area IPS with a single generating unit using a hybrid NN-FTF controller. For a two-area, nonlinear IPS with non-reheat thermal and hydro units, an SA-based PID controller was also presented [25]. Moreover, relevant work on IPSs presented by different authors can be seen in [26–28].There is extensive research in the field of individual LFCs. Recently published work in the field of LFC can be found in [29–33]. The nomenclature used in this work is provided in Table 1, while the summary of the literature studies on the combined control of LFC-AVR loops is shown in Table 2.

In the previous studies, PID and various modified forms of PID such as PIDA, PIDF, PID^{u}F, FOPID, etc., have been used for the combined analysis of AVR and LFC control loops in multi-area, multi-source IPS. The optimal parameters of the controllers were found using various meta-heuristic computational algorithms. Researchers are still searching for new, nature-inspired algorithms as they have recognized their excellent optimization capabilities in various engineering problems. Due to their more complicated system structure, nonlinear systems in particular are difficult to optimize, and they require intelligent control

systems that can find the best global solutions to problems. In the recent past, several novel meta-heuristic computational algorithms have been presented, such as artificial rabbits optimization [34], the dandelion optimizer [35], the sea-horse optimizer [36], the Archimedes optimization algorithm (AOA) [37], the transient search algorithm [38], learner performance-based behavior optimization (LPBO) [39], etc. From a literature survey, it is understood that dandelion optimizers (Dos) have not been employed in multi-area, multi-source IPS. Due to this, DO-based PI-PD controllers for multi-area, multi-source IPS with nonlinearities were investigated in this study. This work's key contributions are:

1. AVR-LFC control loops modeling for a two-area IPS without nonlinearities.
2. AVR-LFC control loops modeling for a two- and three-area realistic IPS with nonlinearities such as GRC, GDB and BD.
3. The design of a PI-PD controller with dandelion optimizer (DO)-based tuning methodology.
4. The performance evaluation and supremacy of a DO-based PI-PD were demonstrated with other control schemes such as HAEFA Fuzzy PID [3], AOA, MPSO and LPBO-based PI-PD.
5. The study of the proposed DO-based control methodology was conducted in a realistic environment with different nonlinearities for a two- and three-area multi-source IPS to demonstrate its effectiveness.

Table 1. Nomenclature.

Acronym	Definition	Acronym	Definition
DO	Dandelion Optimizer	SMES	Superconducting Magnetic Energy Storage
GRC	Generation Rate Constraint	PD	Proportional Derivative
PI	Proportional Integral	AVR	Automatic Voltage Regulator
V_t	Terminal Voltage	B	Area Bias Factor
CES	Capacitive Energy Storage	FESS	Flywheel Energy Storage System
SLP	Step Load Perturbation	UC	Ultra-Capacitors
PID	Proportional Integral Derivative	ΔP_D	Load Deviation
LPBO	Learner Performance-Based Behavior Optimization	MPSO	Modified Particle Swarm Optimization
Δf	Frequency Deviation	RFB	Redox Flow Battery
IPFC	Interline Power Flow Controller	PI-PD	Proportional Integral-Proportional Derivative
BD	Boiler Dynamics	HAEFA	Hybridized Approach of the Artificial Electric Field Algorithm
LFC	Load Frequency Control	PIDA	Accelerated Proportional Integral Derivative
AFA	Artificial Flora Algorithm	UPFC	Unified Power Flow Controller
AOA	Archimedes Optimization Algorithm	GDB	Governor Dead Band
ΔP_{tie}	Tie-Line Power Deviation	R_i	Speed Regulation
ΔX_G	Valve Position of Governor	ΔP_G	Deviation in the Output of Generator
DPO	Doctor and Patient Optimization	IPS	Interconnected Power System
T_{gr}	Time Constant of Speed Governor	T_{CD}	Compressor Discharge Volume Time Constant
K_{re}	Gain of Reheat Steam Turbine	K_p	Gain of Power System
T_{re}	Time Constant of Reheat Steam Turbine	T_p	Time Constant of Power System
T_{tr}	Time Constant of Thermal Turbine	K_a	Gain of Amplifier
T_h	Main Servo Time Constant	T_a	Time Constant of Amplifier
T_{rs}	Speed Governor Rest time	K_e	Gain of Exciter
T_{rh}	Transient droop Time Constant	T_e	Time Constant of Exciter
T_w	Water Time Constant	K_g	Gain of Generator Field
X	Speed Governor Lead Time Constant	T_g	Time Constant of Generator Field
Y	Speed Governor Lag Time Constant	K_s	Gain of Voltage Sensor
a,b,c	Valve Positional Time Constant	T_s	Time Constant of Voltage Sensor
T_{CR}	Combustion Reaction Time Delay	T_f	Fuel Time Constant

Table 2. Literature summary of combined LFC-AVR studies.

Reference	Year	Research Area	Controller	Tuning Method	Covered Area	Generation Sources in All Areas	Generation Sources	Nonlinearities	Additional Incorporation for Improvements
[3]	2022	AVR with LFC	Fuzzy PID	HAEFA	2	6	Reheat thermal, hydro, gas	-	UCs, SMES, RFBs
[4]	2022	AVR with LFC	PI-PD	AOA, LPBO, MPSO	2 3	2 and 3	-	-	-
[5]	2022	AVR with LFC	PIDA	DPO	2	10	Three bioenergy technologies and two solar energy sources	-	-
[6]	2022	AVR with LFC	CPDN-FOPIDN	AFA	3	6	Reheat thermal, hydro, gas and geothermal	GRC, GDB	RFBs, CES, SMES, FESS, HVDC link
[7]	2022	AVR with LFC	CFOTDN-FOPDN	AFA	2	4	Hydro and dish-Stirling, Reheat thermal and solar thermal	GDB, CTD, GRC	-
[8]	2022	AVR with LFC	CFPD-TID	AFA	3	6	Thermal, hydro and geothermal	GDB, GRC	RFBs, HVDC link
[9]	2022	AVR with LFC	2DOF I-TDF	HHO	3	6	reheat thermal, wind, dish-Stirling and solar thermal	GRC, GDB	-
[10]	2022	AVR with LFC	ADRC	2nd order error-driven control law	3	6	Solar, geothermal, wind and EVs	-	-
[11]	2021	AVR with LFC	TIDF	HHO	3	6	Combined cycle gas turbine (CCGT) and reheat thermal	GDB, GRC, BD	-
[12]	2021	AVR with LFC	PIDA	hFPAPFA	1	1	Thermal	-	-
[13]	2021	AVR with LFC	PID	FA	2	4	Reheat thermal and hydro	TD, GRC, GDB	-
[14]	2021	AVR with LFC	PIDD	GWO	2	6	Reheat thermal, hydro and nuclear	GRC, GDB	SMES, UPFC
[15]	2021	AVR with LFC	PID	NLTA	2	2	-	-	-
[16]	2020	AVR with LFC	PIDF, PI	SCA	2	2	Reheat thermal and non-reheat thermal	-	UPFC, RFBs
[17]	2020	AVR with LFC	PID	DE-AEFA	2	6	Gas, diesel, hydro, solar photovoltaic, reheat thermal and wind	GRC	IPFC, RFBs
[18]	2020	AVR with LFC	PID	DE-AEFA	2	6	Wind, hydro, thermal, gas, solar and diesel	GRC	HVDC link
[19]	2020	AVR with LFC	CPSS	IPSO	1	1	Gas, reheat thermal and hydro	GDB, GRC	-
[20]	2019	AVR with LFC	PID	FA	2	4	Hydro and non-reheat thermal	-	-
[21]	2019	AVR with LFC	FOPID	MFO	2	4	Hydro and non-reheat thermal	GDB, BD	-

Table 2. *Cont.*

Reference	Year	Research Area	Controller	Tuning Method	Covered Area	Generation Sources in All Areas	Generation Sources	Nonlinearities	Additional Incorporation for Improvements
[22]	2018	AVR with LFC	PIDF, PID^{u}F	LSA	2	4	Reheat thermal, wind and diesel	GDB, GRC	IPFC, SMES
[23]	2018	AVR with LFC	PID, Fuzzy	ZN, FLC	1	1	-	-	-
[24]	2016	AVR with LFC	Hybrid NN and FTF	NN-FTF	1	1	-	-	-
[25]	2016	AVR with LFC	PID	SA, ZN	2	4	Hydro and non-reheat thermal	GDB	-
Proposed Method	2022	AVR with LFC	PI-PD	DO, AOA, LPBO, MPSO	2 and 3	6 and 9	Thermal, gas and hydro	GDB, GRC, BD	-

The present work is organized as follows: The modeling of the power system is presented in Section 2. Section 3 contains a description of the proposed methodology. The details of the proposed dandelion optimizer are presented in Section 4. Section 5 discusses the implementation of the proposed approach and the results. Finally, Section 6 summarizes the conclusions and future recommendations.

2. System Modeling

The multi-area, multi-source IPS model with combined AVR-LFC loops under study is shown in Figure 1. It consists of multiple areas with gas, hydro and thermal reheat systems identical in each area [3]. Figure 1a represents the model of a single-area IPS, whereas the tie-line connections are demonstrated in Figure 1b [3].

The LFC loop of ith area has a controller $K_{LFC}(s)$, ith area's bias factor (B_i), thermal reheat speed regulation (R_t), hydro speed regulation (R_h), gas speed regulation (R_g) and generator/load ($\frac{K_{p(i)}}{sT_{p(i)}+1}$) with different blocks of power generation units. The thermal reheat unit consists of thermal governor ($\frac{1}{sT_{gr}+1}$), reheat turbine ($\frac{K_{re}T_{re}}{sT_{re}+1}$) and thermal turbine ($\frac{1}{sT_{tr}+1}$); hydro unit includes hydro governor ($\frac{1}{sT_h+1}$) and transient droop compensation ($\frac{sT_{rs}+1}{sT_{rh}+1}$), hydro turbine ($\frac{1-sT_w}{1+0.5T_ws}$); gas unit comprises gas governor ($\frac{Xs+1}{Ys+1}$), valve position ($\frac{a}{bs+c}$), fuel system ($\frac{1-sT_{CR}}{1+sT_f}$) and compressor discharge system ($\frac{1}{sT_{CD}+1}$). $\Delta P_{D(i)}$, $\Delta f_{(i)}$, $\Delta V_{t(i)}$ and $\Delta P_{tie(i)}$ denote the load deviation, frequency deviation, deviation in terminal voltage and tie-line power deviation respectively. $V_{t(i)}$, $V_{e(i)}$, $V_{ref(i)}$ and $V_{s(i)}$ refer to the terminal voltage, error voltage, reference voltage and sensor voltage in ith area respectively. The purpose of tie-line connection is to interconnect multiple areas in an IPS. The AVR loop of ith area consists of a controller ($K_{AVR}(s)$), amplifier ($\frac{K_{a(i)}}{sT_{a(i)}+1}$), generator ($\frac{K_{g(i)}}{sT_{g(i)}+1}$), exciter ($\frac{K_{e(i)}}{sT_{e(i)}+1}$), and sensor ($\frac{K_{s(i)}}{sT_{s(i)}+1}$). K_1, K_2, K_3, K_4 and P_s are the coefficients for mutual coupling between AVR and LFC loops. The synchronization coefficient between ith and jth area is represented by T_{ij}. The transfer function models of the reheat thermal ($G_T(s)$), gas ($G_G(s)$) and hydro ($G_H(s)$) systems provided in Equations (1)–(3) respectively [3]. The definitions of all terms used in Equations (1)–(3) are provided in Table 1.

$$G_T(s) = \frac{1 + T_{re}K_{re}s}{(1 + T_{gr}s)(1 + T_{re}s)(1 + T_{tr}s)} \tag{1}$$

$$G_G(s) = \frac{(1 + Xs)(1 - T_{CR}s)a}{(1 + Ys)(c + bs)(1 + T_fs)(1 + T_{CD}s)} \tag{2}$$

$$G_H(s) = \frac{(1 + T_{rs}s)(1 - T_ws)}{(1 + T_hs)(1 + T_{rh}s)(1 + 0.5T_ws)} \tag{3}$$

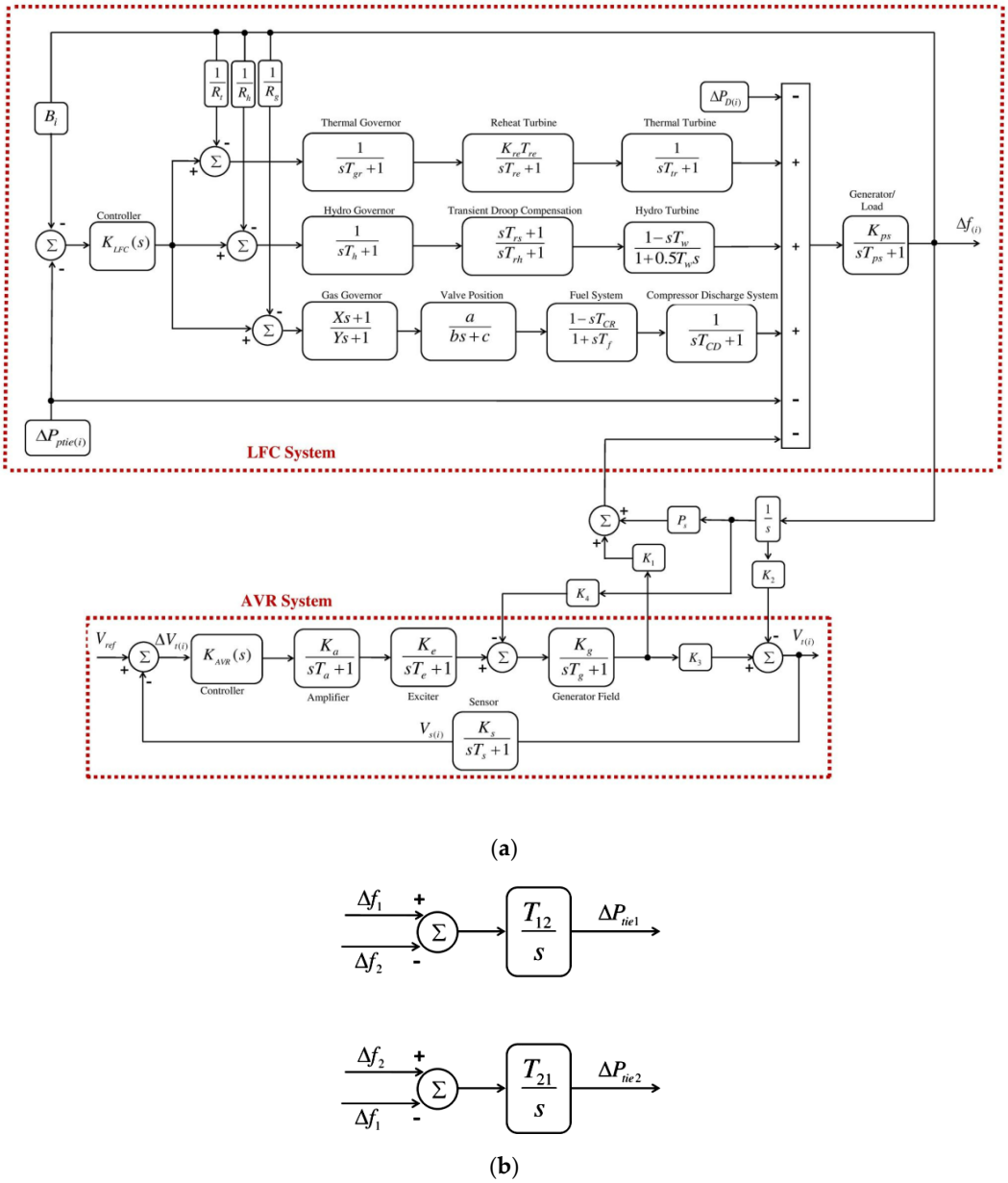

(**a**)

(**b**)

Figure 1. (**a**) Model of IPS with combined AVR-LFC. (**b**) Tie-ine connection for two-area.

The AVR loop comprises a sensing unit, an exciter, a generator, an amplifier and a controller ($K_{2(i)}(s)$). The sensor continuously senses the terminal voltage and provides the error voltage signal after comparing it with the reference voltage. The controller generates the signal for the amplifier from the error signal. The amplified signal is then given to the excitation unit to control the field excitation.

2.1. Power System with Nonlinearities

Several nonlinearities, including GRC, GDB and BD, were included in the multi-area multi-source IPS to increase the realism of the system. In this section, the details of each nonlinear component of the existing power system are explained.

2.1.1. Generation Rate Constraint (GRC)

The steam turbine is subject to thermodynamic and mechanical constraints, which are the main causes of GRC. The saturation type nonlinearity is used to characterize GRC, which fundamentally limits the steam turbine. The modeling of the power system must

take this limitation into account; otherwise, the system is likely to be subjected to severe turbulence leading to governor wear. The GRC of a thermal power plant is often lower than that of a hydroelectric plant. For a hydropower plant, the GRC is 360%/min for lower generation and 270%/min for higher generation. For a thermal power plant, the GRC is an upper limit of +3%/min and a lower limit of −3%/min [40].

2.1.2. Governor Dead Band (GDB)

The GDB is the measure of the total steady-state velocity variations that do not change the governor valve. The GDB is always defined as a percentage of the rated speed and reflects the insensitivity of the speed control mechanism. In this work, the value of GDB is assumed to be ±0.036%. GDB causes oscillations in the system and increases the perceived inaccuracy in a steady state. To express the GDB and its transfer function model, the backlash form of nonlinearity is used [41].

2.1.3. Boiler Dynamics (BD)

The model of the transfer function of the boiler dynamics is shown in Figure 2. Combustion control is included in this model. The model can be used to study coal-fired plants with well-tuned combustion control as well as oil- or gas-fired plants with poor combustion control. Typical steam plants use turbine control valves to initiate changes in generation, and when the boiler control system detects changes in pressure deviations and the steam flow rate, the necessary controls are immediately applied [30,42].

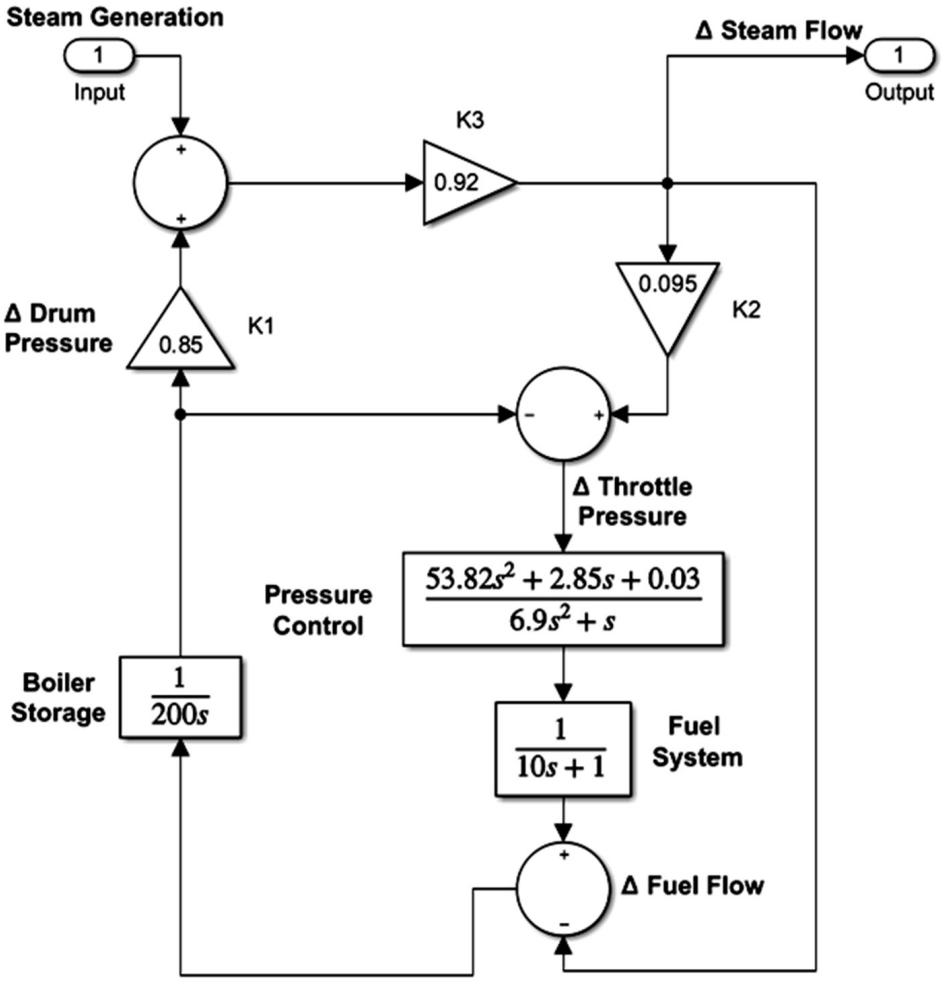

Figure 2. Transfer function model boiler dynamics [42].

3. Proposed Methodology

PID controllers are often used in industrial applications because of their simpler design and implementation. PID controllers often operate effectively, although modified PID control structures have been shown to perform better in combined AVR-LFC interconnected power systems [4]. Modified forms of PID, such as PI-PD, have been developed to achieve the best transient and steady-state response while eliminating system errors [43]. The PD component, which is in the feedback path, is not affected by an abrupt change in the set point. The controller component in the feedback path can significantly increase the closed-loop response. In the forward path is the PI portion of the PI-PD, which responds directly to error signals coming from the summing junction. Recently, a PI-PD controller has been effectively used in a variety of applications [44–50]. Figure 3 illustrates the suggested control scheme with IPS. The following summarizes the PI-PD controllers' transfer function model:

$$U(s) = (K_{p1} + \frac{K_i}{s})E(s) - (K_{p2} + K_d s)Y(s) \quad (4)$$

where $U(s)$ and $E(s)$ represent control and error signals, respectively.

The error signal can be expressed as

$$E(s) = Y(s) - R(s) \quad (5)$$

where $R(s)$ and $Y(s)$ depict reference and output signals, respectively.

The cost function (J) is optimized to determine the ideal controller parameters using nature-inspired computational strategies.

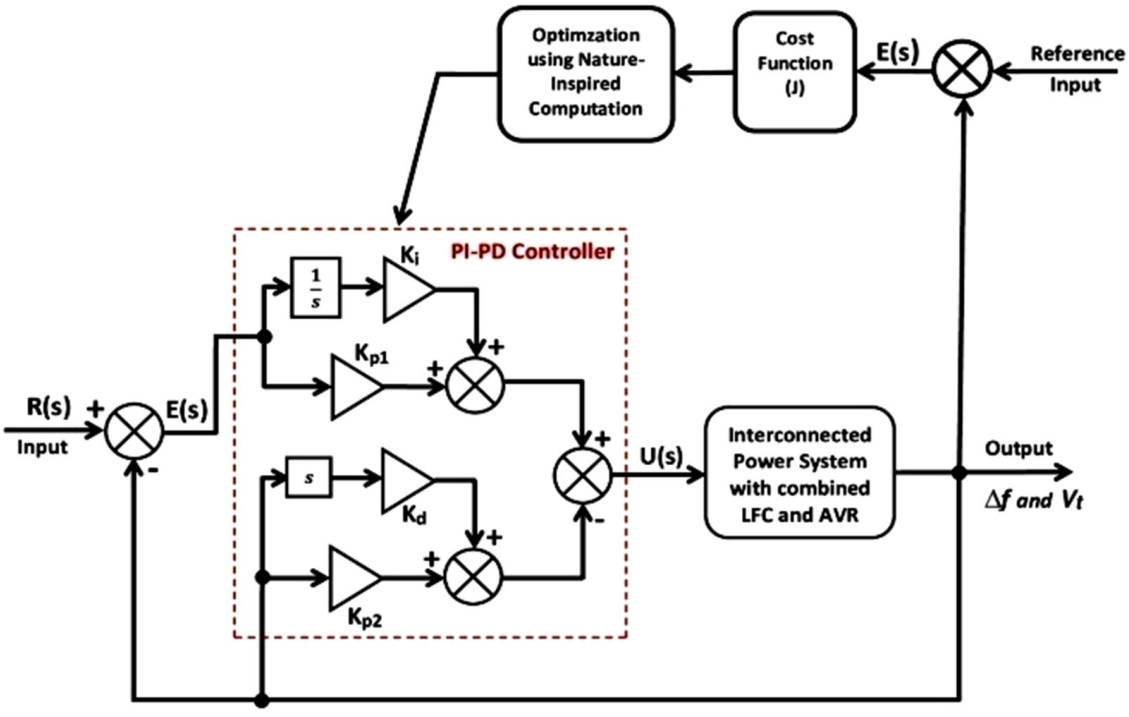

Figure 3. Proposed control scheme [4].

The following equations represent various performance indices that can be used to optimize error signal, including the integral of the squared value of error (ISE), the integral of time multiplied with the absolute value of error (ITAE), the integral of the absolute value of error (IAE) and the integral of time multiplied with the squared value of error (ITSE) [4].

$$J_{\text{ISE, two-area}} = \int_0^T \left(\Delta f_1^2 + \Delta f_2^2 + \Delta V_{t1}^2 + \Delta V_{t2}^2 + \Delta P_{tie12}^2\right) dt \quad (6)$$

$$J_{\text{IAE, two-area}} = \int_0^T (|\Delta f_1| + |\Delta f_2| + |\Delta V_{t1}| + |\Delta V_{t2}| + |\Delta P_{tie12}|)dt \quad (7)$$

$$J_{\text{ITSE, two-area}} = \int_0^T t\left(\Delta f_1^2 + \Delta f_2^2 + \Delta V_{t1}^2 + \Delta V_{t2}^2 + \Delta P_{tie12}^2\right)dt \quad (8)$$

$$J_{\text{ITAE, two-area}} = \int_0^T t(|\Delta f_1| + |\Delta f_2| + |\Delta V_{t1}| + |\Delta V_{t2}| + |\Delta P_{tie12}|)dt \quad (9)$$

For a three-area IPS, we can write

$$J_{\text{ISE, three-area}} = \int_0^T \left(\Delta f_1^2 + \Delta f_2^2 + \Delta f_3^2 + \Delta V_{t1}^2 + \Delta V_{t2}^2 + \Delta V_{t3}^2 + \Delta P_{tie1}^2 + \Delta P_{tie2}^2 + \Delta P_{tie3}^2\right)dt \quad (10)$$

$$J_{\text{IAE, three-area}} = \int_0^T (|\Delta f_1| + |\Delta f_2| + |\Delta f_3| + |\Delta V_{t1}| + |\Delta V_{t2}| + |\Delta V_{t3}| + |\Delta P_{tie1}| + |\Delta P_{tie2}| + |\Delta P_{tie3}|)dt \quad (11)$$

$$J_{\text{ITSE, three-area}} = \int_0^T t\left(\Delta f_1^2 + \Delta f_2^2 + \Delta f_3^2 + \Delta V_{t1}^2 + \Delta V_{t2}^2 + \Delta V_{t3}^2 + \Delta P_{tie1}^2 + \Delta P_{tie2}^2 + \Delta P_{tie3}^2\right)dt \quad (12)$$

$$J_{\text{ITAE, three-area}} = \int_0^T t(|\Delta f_1| + |\Delta f_2| + |\Delta f_3| + |\Delta V_{t1}| + |\Delta V_{t2}| + |\Delta V_{t3}| + |\Delta P_{tie1}| + |\Delta P_{tie2}| + |\Delta P_{tie3}|)dt \quad (13)$$

where

$$\begin{aligned} \Delta V_{t1} &= V_{ref} - V_{t1} \\ \Delta V_{t2} &= V_{ref} - V_{t2} \\ \Delta V_{t3} &= V_{ref} - V_{t3} \end{aligned} \quad (14)$$

$$\begin{aligned} \Delta P_{ptie1} &= \Delta P_{ptie12} + \Delta P_{ptie13} \\ \Delta P_{ptie2} &= \Delta P_{ptie21} + \Delta P_{ptie23} \\ \Delta P_{ptie3} &= \Delta P_{ptie31} + \Delta P_{ptie32} \end{aligned} \quad (15)$$

Due to excellent convergence and performance characteristics, ITSE is used as the error criterion in this work to minimize the cost function (J).

4. Nature-Inspired Computation Algorithms

Nature-inspired computational algorithms capable of handling complex engineering problems have attracted much attention in interconnected power systems. The dandelion optimizer (DO) has been used to find the optimal parameters of the controller. The control scheme provides the most suitable controller parameters when the cost function is minimized. In this study, an attempt is made to improve the LFC and AVR response in a multi-area, multi-source IPS by using nature-inspired computational control methods.

Dandelion Optimizer (DO)

In 2022, Shijie Zhao proposed the algorithm known as the dandelion optimizer (DO), which takes inspiration from nature. A dandelion is a plant that uses wind to spread its seeds [35]. The three stages that dandelion seeds go through are listed below:

1. A vortex is formed above the dandelion seed during the rising stage, and it rises while being propelled higher by wind and sunlight. In contrast, there are no eddies above the seeds on a rainy day. In this situation, only local searches are possible.
2. When seeds reach a specific height during the descending stage, they begin to steadily sink.
3. Dandelion seeds finally randomly land in one location during the landing stage, where they will develop new dandelions as a result of the influence of the wind and weather.

By dispersing their seeds to the next generation, dandelions evolve their population based on the following three stages.

Stage 1: Initialization

Each dandelion seed in the DO algorithm indicates a potential solution. The population of a DO can be expressed as:

$$population = \begin{bmatrix} x_1^1 \ldots\ldots\ldots\ldots\ldots x_1^{Dim} \\ \ldots \\ \ldots \\ x_{pop}^1 \ldots\ldots\ldots\ldots\ldots x_{pop}^{Dim} \end{bmatrix} \tag{16}$$

where *pop* and *Dim* stand in for the population size and the dimension of the variable, respectively.

Between the specified problem's upper bound (*UB*) and lower bound (*LB*), each possible solution is produced at random, and the *i*th individual X_i can be expressed as

$$X_i = rand \times (UB - LB) + LB \tag{17}$$

where i is an integer between 1 and pop, whereas rand represents a random number between 0 and 1.

UB and *LB* can be written as:

$$\begin{array}{c} LB = [lb_1, \ldots\ldots\ldots, lb_{Dim}] \\ UB = [ub_1, \ldots\ldots\ldots, ub_{Dim}] \end{array} \tag{18}$$

According to DO, the initial elite is the individual with the highest fitness value, which is referred to as the best position for the dandelion seed to grow. The initial elite's mathematical formulation, using the minimal value as an illustration, is

$$\begin{array}{l} f_{best} = \min(f(X_i)) \\ X_{elite} = X(find(f_{best} == f(X_i))) \end{array} \tag{19}$$

where *find*() represents two indices having the same values.

Stage 2: Rising stage

In order to float away from their parent plants, dandelion seeds must reach a specific height during the rising stage. Dandelion seeds rise to various heights depending on air humidity, wind speed, etc. The two weather conditions in this instance are as follows.

Case 1:

Wind speeds on a clear day can be thought of as having a lognormal distribution, $\ln Y \sim N(\mu, \sigma^2)$. The wind speed affects how high a dandelion seed will rise. If the wind is stronger, the dandelion flies higher, and the seeds scatter farther.

$$X_{t+1} = X_t + \alpha \times v_x \times v_y \times \ln Y \times (X_s - X_t) \tag{20}$$

where X_s shows the randomly selected position at iteration t, and X_t shows the dandelion seed's position at iteration t.

Equation (21) shows the expression for the randomly generated position:

$$X_s = rand(1, Dim) \times (UB - LB) + LB \tag{21}$$

ln$Y$ shows a lognormal distribution subject to μ = 0 and σ^2 = 1.

$$\ln Y = \left\{ \begin{array}{l} \frac{1}{y\sqrt{2\pi}} \exp[-\frac{1}{2\sigma^2}(\ln y)^2] \\ 0 \end{array} \right\} \begin{array}{l} y \geq 0 \\ y < 0 \end{array} \tag{22}$$

where y indicates the standard normal distribution (0, 1).

$$\alpha = rand() \times (\frac{1}{T^2}t^2 - \frac{2}{T}t + 1) \tag{23}$$

where

α represents a random perturbation between [0, 1];
v_x and v_y demonstrate the dandelion's lift component coefficients.

$$\begin{array}{l} r = \frac{1}{e^{\theta}} \\ v_x = r\cos\theta \\ v_y = r\sin\theta \end{array} \tag{24}$$

where θ varies randomly between $[-\pi, \pi]$.

Case 2:

Due to humidity and air resistance, dandelion seeds struggle to rise properly with the wind on a wet day.

$$\begin{array}{l} X_{t+1} = X_t \times k \\ k = 1 - rand() * q \end{array} \tag{25}$$

A dandelion uses k to control its local search area. The domain (q) can be obtained using Equation (34) as

$$q = \frac{1}{T^2 - 2T + 1}t^2 - \frac{1}{T^2 - 2T + 1}t + 1 + \frac{1}{T^2 - 2T + 1} \tag{26}$$

The mathematical equation for the dandelion seed's ascending stage is, finally,

$$X_{t+1} = \left\{ \begin{array}{l} X_{t+1} = X_t + \alpha \times v_x \times v_y \times \ln Y \times (X_s - X_t) \\ X_{t+1} = X_t \times k \end{array} \right\} \begin{array}{l} \text{randn} < 1.5 \\ \text{else} \end{array} \tag{27}$$

The random number generated by the function randn() follows the normal distribution.

Stage 3: Descending stage

In this stage, dandelion seeds rise to a particular height and then slowly sink (exploration phase). Brownian motion is employed in DO to replicate the trajectory of a dandelion as it moves.

$$X_{t+1} = X_t - \alpha \times \beta_t \times (X_{mean\_t} - \alpha \times \beta_t \times X_t) \tag{28}$$

where β_t indicates the Brownian motion.

$$X_{mean\_t} = \frac{1}{pop}\sum_{i=1}^{pop} X_i \tag{29}$$

Stage 4: Landing stage

The DO algorithm concentrates on exploitation in this last stage. The dandelion seed makes its landing location at random based on the results of the prior two stages. The algorithm should converge to the optimal solution as the iterations increasingly advance. The population's evolution finally leads to the following global optimal solution:

$$X_{t+1} = X_{elite} + levy(\lambda) \times \alpha \times (X_{elite} - X_t \times \delta) \tag{30}$$

where X_{elite} denotes the seed's optimal position.

$$levy(\lambda) = s \times \frac{w \times \sigma}{|t|^{\frac{1}{\beta}}} \tag{31}$$

The fixed constant for s is 0.01. β is a random number and its values may vary between 0 and 2. t and w are arbitrary numbers in the range [0, 1]. σ is expressed mathematically as follows:

$$\sigma = \left(\frac{\Gamma(1+\beta) \times \sin(\frac{\pi\beta}{2})}{\Gamma(\frac{1+\beta}{2}) \times \sin(\frac{\beta-1}{2})} \right) \tag{32}$$

The value of β is 1.5, and δ can be obtained as:

$$\delta = \frac{2t}{T} \tag{33}$$

The flow chart of the DO algorithm is provided in Figure 4.

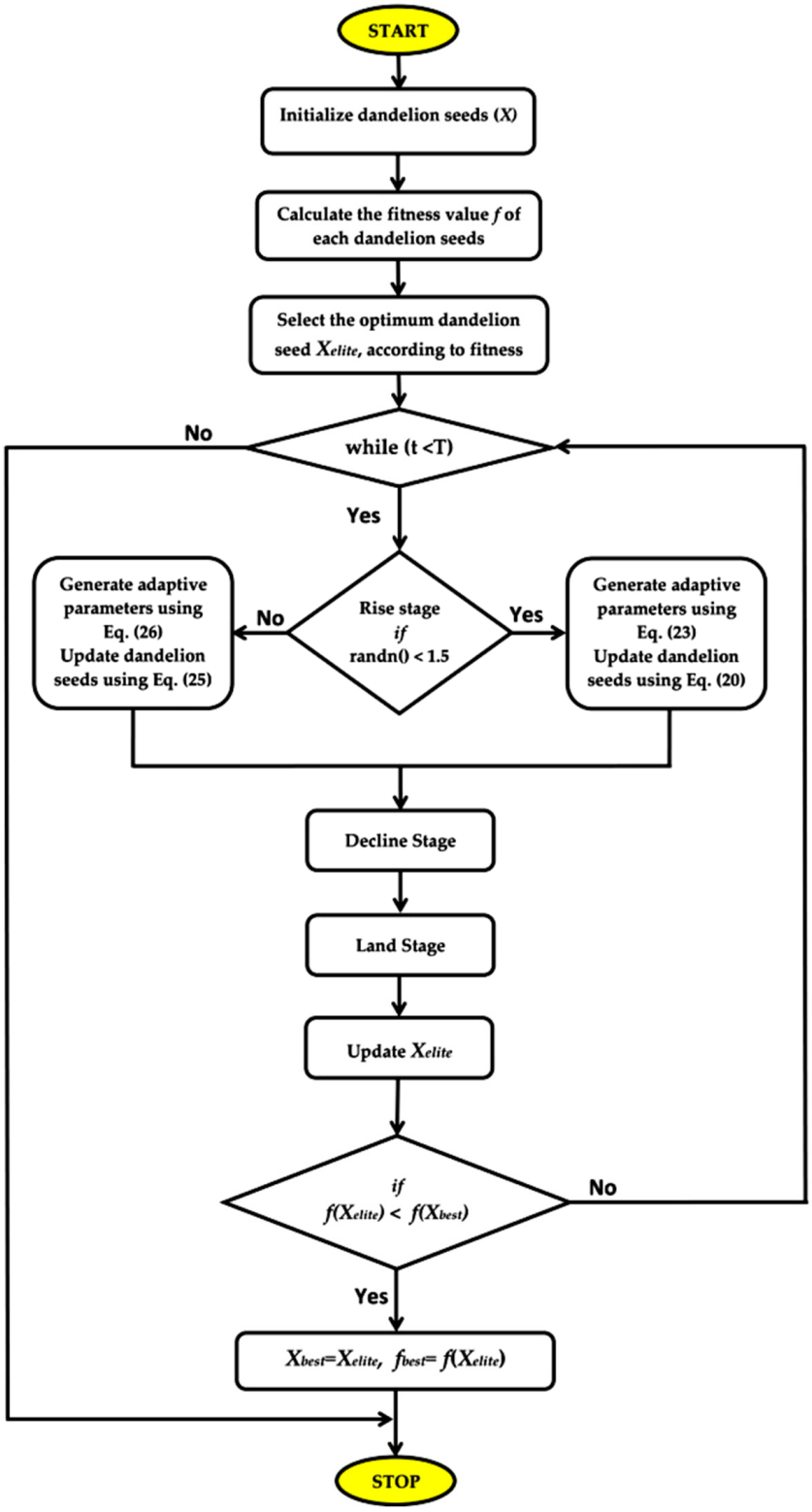

Figure 4. Flow chart of a dandelion optimizer.

5. Implementation and Results Discussion

To express the validation of the proposed control scheme, numerous simulations were performed in MATLAB/Simulink to analyze the results. First, IPS was optimized using AOA, LPBO, MPSO and DO algorithm-based PI-PD control schemes in a two-area multi-source network. In this IPS, both areas had three generating units, including thermal reheat, gas and hydro. The successful results led to applying the proposed methodology to the same IPS with additional nonlinearities such as BD, GDB and GRC. Finally, to confirm the exceptional performance of the proposed scheme, an IPS with a three-area multi-source IPS with nonlinearities was also investigated.

5.1. Frequency and Voltage Stabilization in a Two-Area Multi-Source IPS without Nonlinearities

Figure 5 presents the two-area multi-source IPS model. The system parameters of the two-area IPS are specified in Appendix A. The power system's dynamic analysis was performed using area-1′s laid-out 10% step load perturbation. The parameters of optimization algorithms are provided in Table 3. The optimal parameters of AOA-, LPBO-, MPSO- and DO-based PI-PD control strategies are presented in Table 4. For the sake of assessing the proposed DO-based PI-PD control scheme, the evaluation of the time response of each control scheme was carried out, and comparisons were made with the results of HAEFA Fuzzy PID-, AOA-, LPBO- and MPSO-based PI-PD controllers.

The frequency deviation responses of area-1 and area-2 for a two-area IPS are shown in Figure 6 using the AOA-, LPBO-, MPSO- and DO-based PI-PD control techniques. As can be seen, the frequency deviation response from the suggested control schemes was quite good. For the area-1 LFC, the DO-based PI-PD provided a settling time of 5.44 s, which is lower than other control schemes and, relatively, 53% better than the HAEFA Fuzzy PID controller [3]. Particularly, the AOA- and LPBO-based PI-PDs yielded zero % overshoot. The MPSO-based PI-PD provided a settling time of 5.60 s for area-2 LFC, which is less than other control schemes; that is, it is 32% better than the HAEFA Fuzzy PID controller. The AOA- and LPBO-based PI-PD control schemes provided zero % overshoot in both areas. The steady-state error is always zero when using the suggested methods.

Figure 7 depicts the terminal voltage responses of area-1 and area-2, employing LPBO-, AOA-, MPSO- and DO-based PI-PD control schemes. As can be observed, the terminal voltage response produced by the suggested control strategies was quite excellent. The proposed DO-based PI-PD produced settling times of 1.32 s and 1.40 s in the area-1 and area-2 AVR, which are lower than others. The DO-based PI-PD provided, relatively, a 40% and 31% better AVR settling time response compared with the HAEFA Fuzzy PID controller in the area-1 and area-2 AVR, respectively. The AOA-based PI-PD provided a 0.0020% overshoot in the area-1 AVR, whereas the LPBO-based PI-PD provided 0.016% overshoot in the area-2 AVR. The AOA-based PI-PD yielded, relatively, a 99% better overshoot response in area-1, whereas the LPBO-based PI-PD produced a 99.8% better overshoot response in the area-2 AVR, respectively, compared with the HAEFA Fuzzy PID controller. Furthermore, the steady-state error was zero in each case using the suggested methods.

The numerical results of the frequency deviation, terminal voltage and tie-line power deviation responses employing HAEFA Fuzzy PID-, DO-, AOA-, LPBO- and MPSO-based PI-PD control techniques in a two-area multi-source IPS are presented in Tables 5–7, respectively. Figure 8 depicts the tie-line power deviation response for a two-area IPS with three sources in each area utilizing the AOA-, LPBO- and MPSO- and DO-based PI-PD control schemes. It can be observed that the LPBO-based PI-PD produced a settling time of 3.87 s, which is better than other control schemes; that is, it is 75% relatively better than the HAEFA Fuzzy PID controller. Moreover, each proposed control scheme provided a negligible% overshoot and undershoot responses. With each control scheme, the steady-state error was zero, as can be observed. Figure 9 depicts a graphical comparison of the AOA-, LPBO-, MPSO- and DO-based PI-PD performance characteristics with the HAEFA Fuzzy PID controller in a two-area IPS. In comparison with the HAEFA fuzzy PID controller,

the DO-based PI-PD-based control scheme offered relatively superior frequency, terminal voltage and tie-line power deviation responses.

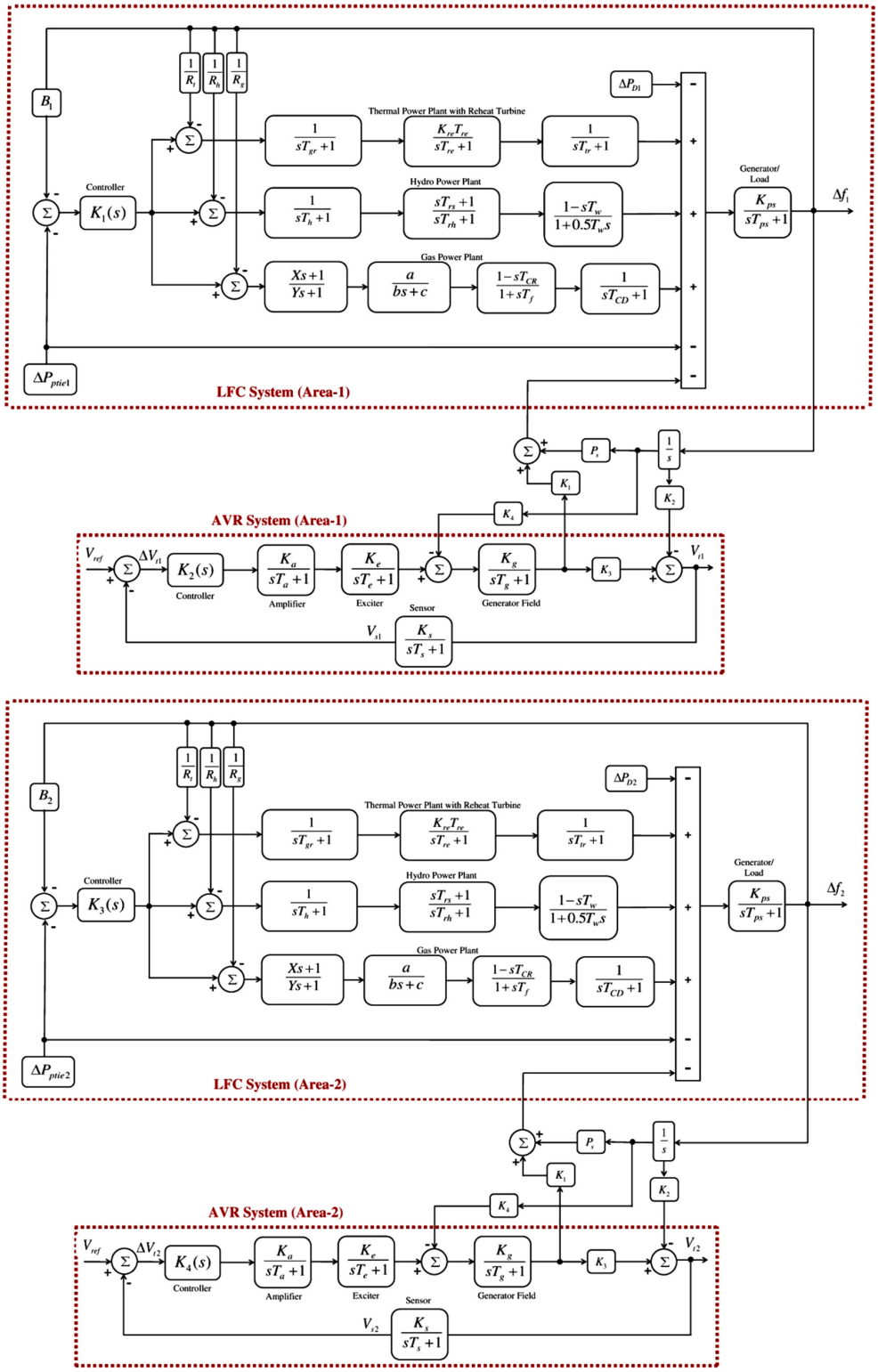

Figure 5. Two-area multi-source IPS.

Table 3. Parameters of optimization algorithms.

AOA		LPBO		MPSO		DO	
Parameter	**Value**	**Parameter**	**Value**	**Parameter**	**Value**	**Parameter**	**Value**
Iterations	4, 6, 4	Iterations	4, 6, 4	Iterations	5, 6, 5	Iterations	5, 6, 5
C_1	2	Crossover Percentage	0.65	Inertia Weight Damping Ratio	1	Lower Bound	0
C_2	6	Mutation Percentage	0.3	Personal Learning Coefficient	2.74	Upper Bound	2
C_3	2	Mutation Rate	0.03	Global Learning Coefficient	2.88	Population Size	20, 10, 20
C_4	0.5	Number of Mutants	6	Max. Velocity Limit	0.2		
Range of Normalization (u,L)	0.9, 0.1	Number of Offspring	14	Min. Velocity Limit	−0.2	-	-
Population Size	25, 10, 25	Population Size	20, 13, 20	Population Size	20, 10, 20	-	-

Table 4. Optimal controller parameters for a two-area multi-source IPS.

Area	Parameters of Controllers	AOA-Based PI-PD	LPBO-Based PI-PD	MPSO-Based PI-PD	DO-Based PI-PD
Area-1	K_{p1}	1.59	1.09	0.46	0.97
	K_{i1}	0.93	1.10	0.78	1.97
	K_{p2}	0.89	1.44	1.14	0.67
	K_{d1}	1.57	1.27	1.47	1.39
	K_{p3}	1.32	1.82	1.06	2
	K_{i2}	1.87	1.22	1.73	1.83
	K_{p4}	1.29	0.35	1.20	0.67
	K_{d2}	0.73	0.42	0.73	0.75
Area-2	K_{p5}	1.59	0.68	1.16	1.03
	K_{i3}	0.94	0.68	0.17	0.23
	K_{p6}	1.13	1.24	0.97	0.73
	K_{d3}	1.34	1.60	1.56	0.92
	K_{p7}	1.82	1.78	1.38	2
	K_{i4}	1.73	1.57	1.60	1.1
	K_{p8}	1.04	0.96	0.98	0.33
	K_{d4}	0.97	0.93	0.66	0.77
	ITSE	0.35	0.28	0.39	0.24

5.2. Frequency and Voltage Stabilization in a Two-Area Multi-Source IPS with Nonlinearities

In this section, the proposed methods are applied to a two-area multi-source IPS, considering nonlinearities such as BD, GRC and GDB. In addition, a dynamic analysis of the power system with a 5% SLP in area-1 and area-2. The model under study is shown in Figure 10, and the parameters of the model are listed in Appendix A.

Table 8 provides the optimum values of AOA-, LPBO-, MPSO- and DO-based PI-PD controllers for a two-area realistic IPS with nonlinearities. Figure 11 shows the frequency deviation response, whereas Table 9 presents the numerical results of a realistic IPS with nonlinearities in two areas, each with three sources, employing DO-, AOA-, LPBO- and MPSO-based PI-PD control schemes. Compared withAOA-, LPBO- and MPSO-based PI-PD control techniques, the DO-based PI-PD control strategy provided a settling time of 7.21 s for the area-1 LFC, which is, comparatively, 0.7%, 13% and 7% better. The AOA-, LPBO- and MPSO-based PI-PD control schemes were outperformed by 11%, 7% and 2%, respectively, in terms of settling time for the area-2 LFC using the DO-based PI-PD. As can be observed, the DO-based PI-PD offers a % overshoot and % undershoot response that is considerably better than others in both areas. Further, it can be seen that for each control scheme, the steady-state error is zero.

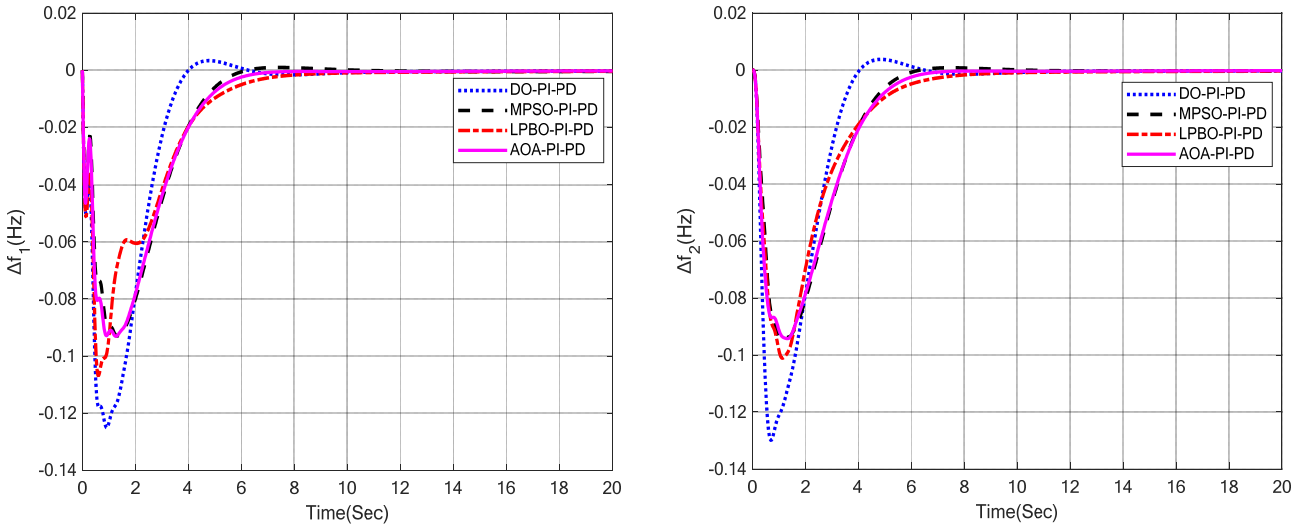

Figure 6. LFC responses in a two-area multi-source IPS with nonlinearities. (**a**) Δf_1; (**b**) Δf_2.

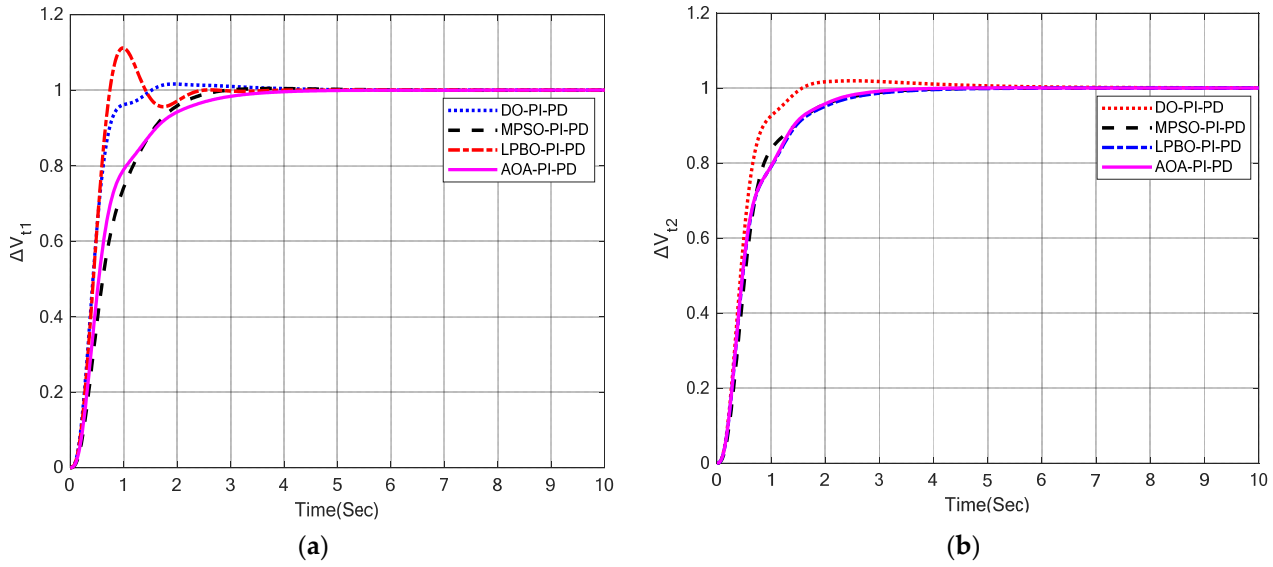

Figure 7. AVR responses in a two-area multi-source IPS. (**a**) V_{t1};(**b**) V_{t2}.

Table 5. Numerical results of an LFC in a two-area multi-source IPS.

Control Scheme	Area-1				Area-2			
	Settling Time	% Overshoot	Undershoot	s-s Error	Settling Time	% Overshoot	Undershoot	s-s Error
AOA-based PI-PD	6.12	0	−0.094	0	6.12	0	−0.094	0
LPBO-based PI-PD	7.14	0	−0.108	0	7.30	0	−0.102	0
MPSO-based PI-PD	5.55	0.001	−0.094	0	5.60	0.001	−0.095	0
DO-based PI-PD	5.44	0.004	−0.126	0	5.61	0.004	−0.130	0

Table 6. Numerical results of an AVR in a two-area multi-source IPS.

Control Scheme	Area-1			Area-2		
	Settling Time	% Overshoot	s-s Error	Settling Time	% Overshoot	s-s Error
HAEFA Fuzzy PID [3]	2.21	12	0	2.02	14	0
AOA-based PI-PD	2.85	0.0020	0	2.45	0.040	0
LPBO-based PI-PD	2.10	10.80	0	2.66	0.016	0
MPSO-based PI-PD	2.30	0.43	0	2.60	3.99×10^{-4}	0
DO-based PI-PD	1.32	1.63	0	1.40	1.94	0

Table 7. Numerical results of tie-line power deviation in a two-area multi-source IPS.

Control Scheme	Settling Time	% Overshoot	Undershoot	s-s Error
HAEFA Fuzzy PID [3]	15.59	0.0005	−0.0035	0
AOA-based PI-PD	12.80	0.0023	−0.021	0
LPBO-based PI-PD	3.87	0.027	−0.057	0
MPSO-based PI-PD	13.69	0.00125	−0.022	0
DO-based PI-PD	8.84	0.006	−0.0235	0

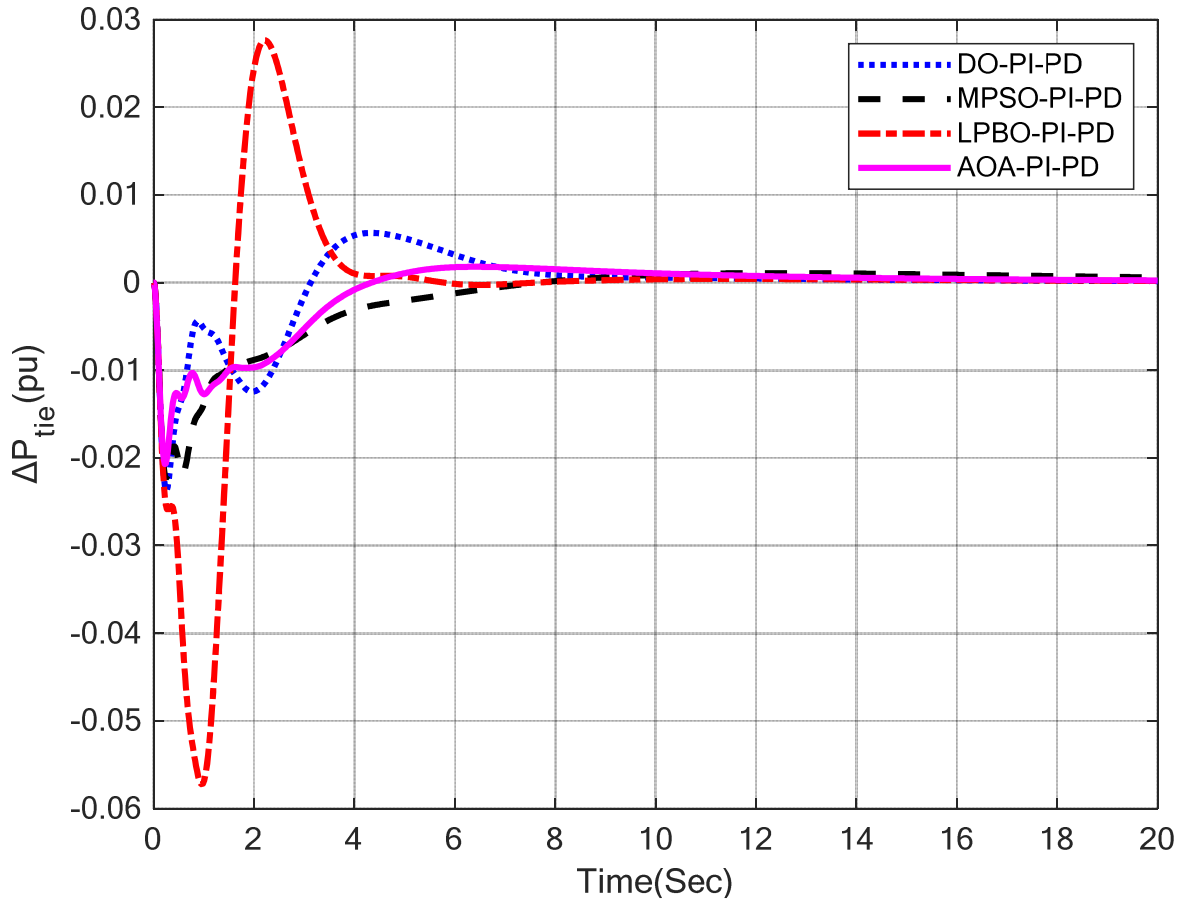

Figure 8. Tie-line power deviation responses in a two-area multi-source IPS.

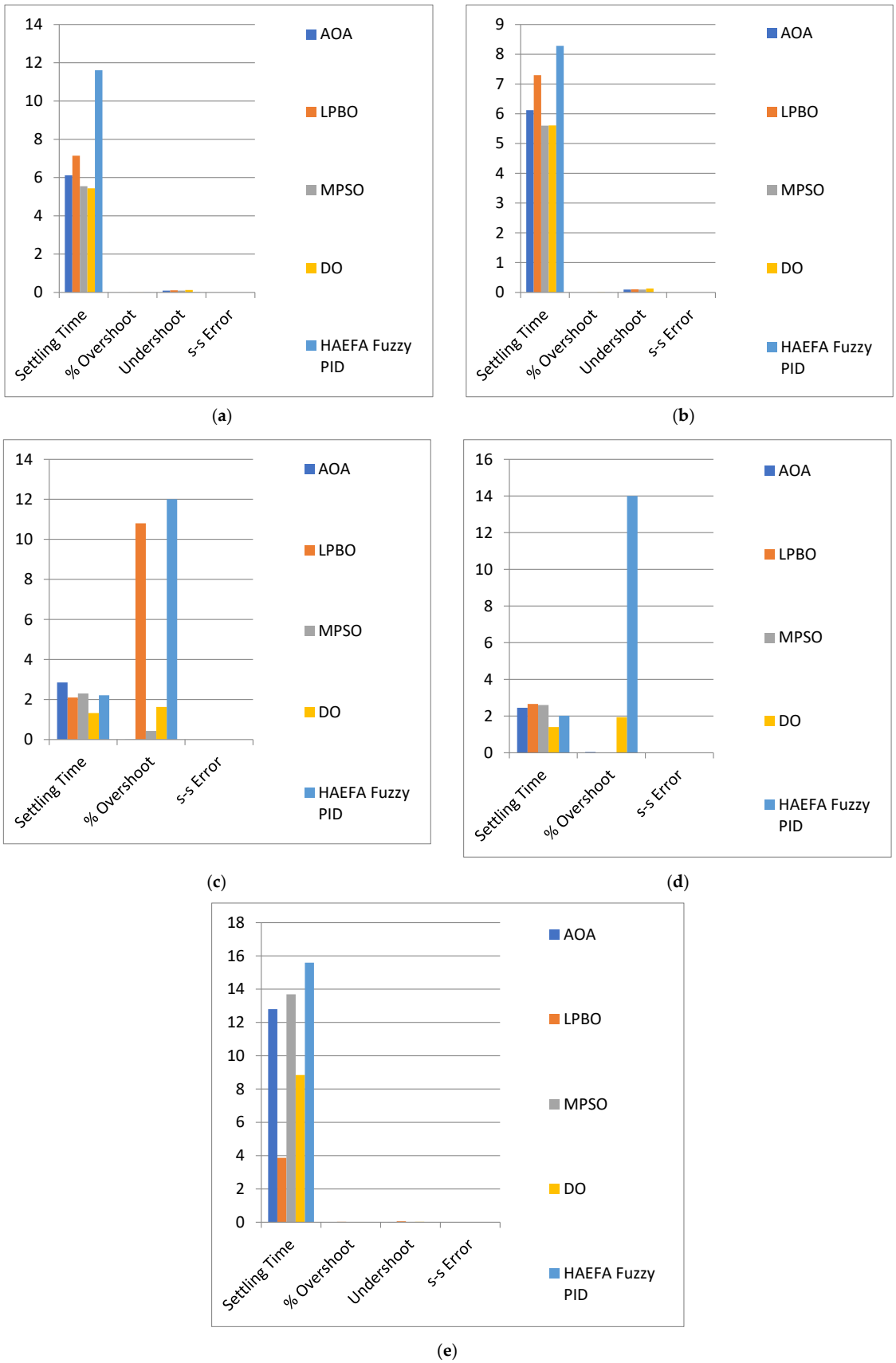

Figure 9. Graphical comparison in a two-area multi-source IPS. (**a**) Δf_1; (**b**) Δf_2; (**c**) V_{t1}; (**d**) V_{t2}; (**e**) $P_{tie\text{-}line}$.

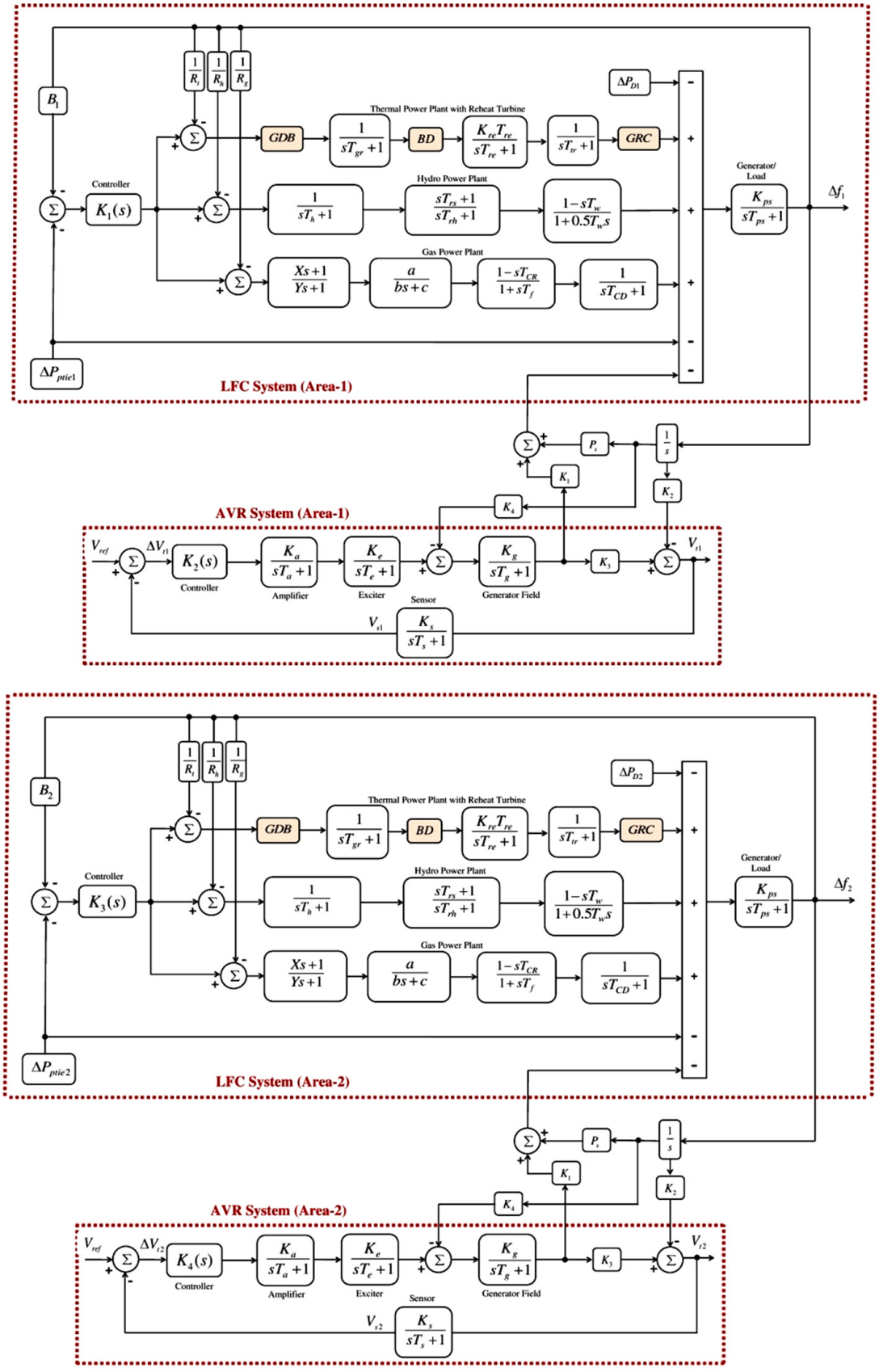

Figure 10. Two-area multi-source realistic IPS with nonlinearities.

Table 8. Optimum controller parameters in a two-area multi-source realistic IPS with nonlinearities.

Area	Parameters of Controllers	AOA-Based PI-PD	LPBO-Based PI-PD	MPSO-Based PIPD	DO-Based PI-PD
Area-1	K_{p1}	0.24	0.0069	0.40	1.05
	K_{i1}	0.20	0.10	1.24	1.74
	K_{p2}	0.65	1.46	0	0.63
	K_{d1}	0.95	1.76	0.89	2
	K_{p3}	1.66	1.91	1.34	1.92
	K_{i2}	1.62	1.52	1.82	1.98
	K_{p4}	0.75	0.94	0.91	1.32
	K_{d2}	1.68	1.42	0.32	0.92
Area-2	K_{p5}	0.87	1.49	1.49	1.14
	K_{i3}	0.66	0.68	0.85	1.21
	K_{p6}	1.84	1.72	1.68	1.17
	K_{d3}	1.86	0.53	0.40	1.77
	K_{p7}	1.31	1.17	1.94	1.37
	K_{i4}	1.16	1.73	1.70	0.80
	K_{p8}	0.37	1.68	1.59	0.39
	K_{d4}	0.28	0.31	1.48	0.62
	ITSE	0.48	0.43	0.45	0.35

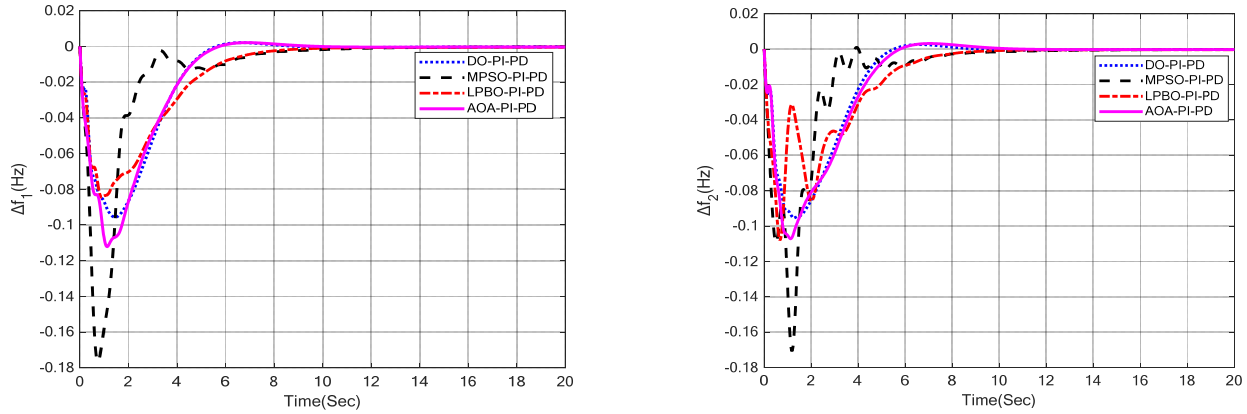

Figure 11. LFC responses in a two-area multi-source realistic IPS with nonlinearities. (**a**) Δf_1; (**b**) Δf_2.

Table 9. Numerical results of LFC in a two-area multi-source realistic IPS with nonlinearities.

Control Scheme	Area-1				Area-2			
	Settling Time	% Overshoot	Undershoot	s-s Error	Settling Time	% Overshoot	Undershoot	s-s Error
AOA-based PI-PD	7.26	0.0215	−0.121	0	8.47	0.0318	−0.107	0
LPBO-based PI-PD	8.24	0	−0.0845	0	8.14	0	−0.1079	0
MPSO-based PI-PD	7.72	0	−0.176	0	7.68	0.000975	−0.171	0
DO-based PI-PD	7.21	0.00212	−0.0958	0	7.54	0.0026	−0.0955	0

Table 10 presents the numerical results of terminal voltages utilizing the DO-, AOA-, LPBO- and MPSO-based PI-PD control strategies, while Figure 12 displays the terminal voltage responses in a two-area realistic IPS with nonlinearities. In comparison with AOA-, LPBO- and MPSO-based PI-PD control strategies, the DO-based PI-PD strategy for the area-1 AVR provided a settling time of 3.30 s, which was, respectively, 42%, 32% and 5% superior. As can be seen, the DO-based PI-PD controller offers a relatively superior AVR settling time response in area-2compared with the AOA-, LPBO- and MPSO-based PI-PD controllers by 1%, 51% and 45%, respectively. In both areas, almost zero % overshoot

was produced by DO-based PI-PD. The steady-state error is zero again with each control scheme in the proposed IPS.

Table 10. Numerical results of an AVR in a two-area multi-source realistic IPS with nonlinearities.

Control Scheme	Area-1			Area-1		
	Settling Time	% Overshoot	s-s Error	Settling Time	% Overshoot	s-s Error
AOA-based PI-PD	5.67	10.03	0	2.51	12.90	0
LPBO-based PI-PD	4.83	3.09	0	5.07	1.43×10^{-4}	0
MPSO-based PI-PD	3.48	7.94	0	4.48	0.0025	0
DO-based PI-PD	3.30	0.0015	0	2.48	0.016	0

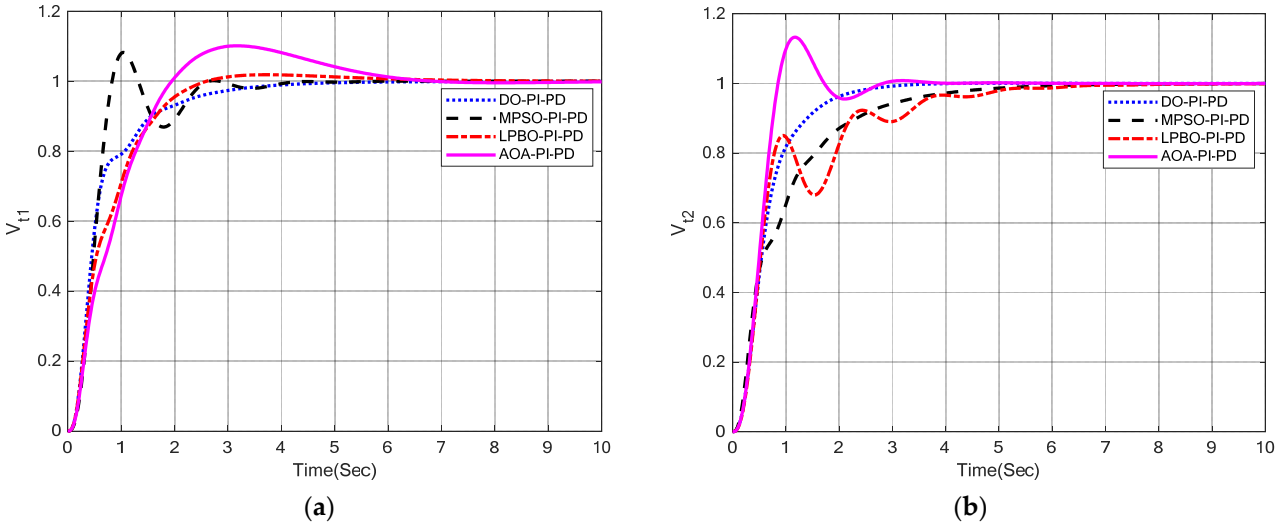

Figure 12. AVR responses in a two-area multi-source realistic IPS with nonlinearities. (**a**) V_{t1}; (**b**) V_{t2}.

Figure 13 shows the tie-line power deviation curves in a two-area realistic IPS with nonlinearities, while Table 11 lists the numerical results of tie-line power deviation responses using the DO-, AOA-, LPBO- and MPSO-based PI-PD control techniques. It is clear that the AOA-, LPBO-, MPSO- and DO-based PI-PD control techniques delivered sufficient tie-line power deviation responses with minimal undershoots and overshoots. The DO-based PI-PD delivered the lowest settling time (8.52 s) in comparison with all other tuning schemes, which is, respectively, 42%, 41% and 9% better than the LPBO-, AOA- and MPSO-based PI-PD control techniques. In comparison to AOA-, LPBO- and MPSO-based PI-PD control strategies, the DO-based PI-PD produced 0.0056% overshoot, which is, comparatively, 66%, 89% and 84% better. It can be seen that the steady-state error is zero for all control schemes.

The performance parameters of the DO-, AOA-, LPBO- and MPSO-based PI-PD control techniques are graphically compared in Figure 14. It is evident that in a two-area IPS with nonlinearities, the PI-PD-based control techniques offer an appropriate transient and steady-state response for terminal voltage, tie-line power deviation and frequency.

5.3. Frequency and Voltage Stabilization in a Three-Area Multi-Source IPS with Nonlinearities

To show the effectiveness of the proposed DO-based PI-PD control scheme, a three-area multi-source IPS with nonlinearities was selected in this section for further investigation. Figure 15 shows the studied model, and Appendix A contains the parameters of the model. In addition, the dynamic analysis of the power system was performed with 2% SLP in area-1, area-2 and area-3. Table 12 shows the optimal parameters of the DO-, AOA-, LPBO- and MPSO-based PI-PD controllers for the three-area IPS with nonlinearities.

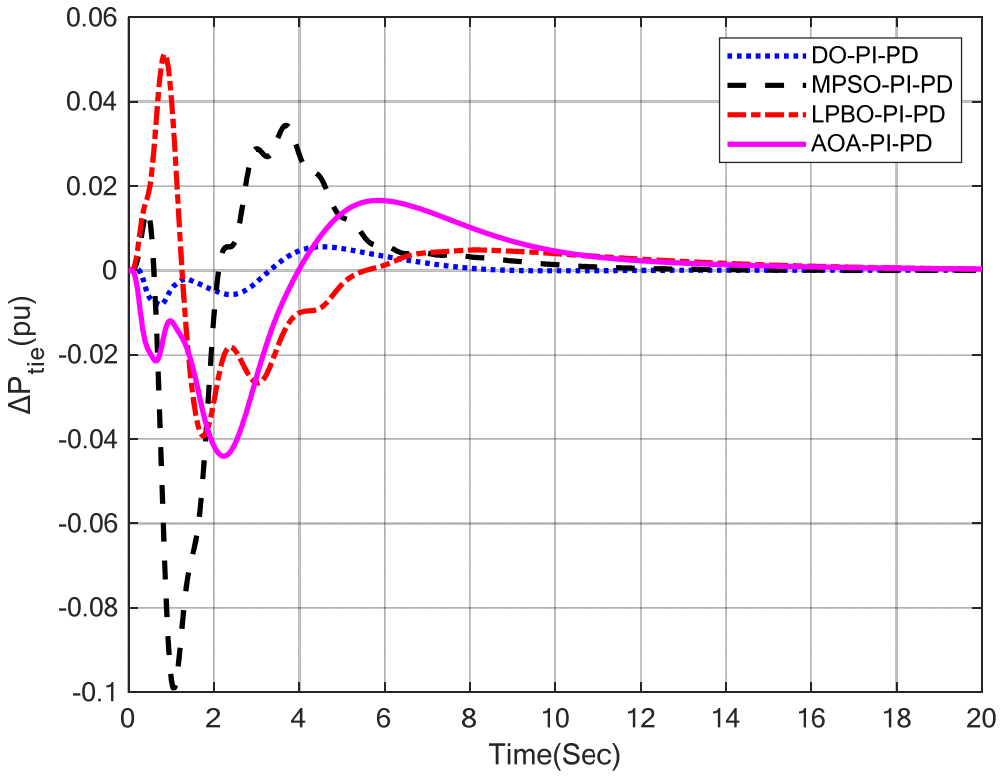

Figure 13. Tie-line power deviation responses in a two-area multi-source realistic IPS with nonlinearities.

Table 11. Numerical results of tie-line power deviation in a two-area multi-source realistic IPS with nonlinearities.

Control Scheme	Settling Time	% Overshoot	Undershoot	s-s Error
AOA-based PI-PD	14.49	0.0166	−0.0441	0
LPBO-based PI-PD	14.58	0.051	−0.0392	0
MPSO-based PI-PD	9.36	0.034	−0.0991	0
DO-based PI-PD	8.52	0.0056	−0.00813	0

Table 13 presents the numerical results of the frequency deviation in a three-area multi-source IPS and nonlinearities utilizing the AOA-, LPBO-, MPSO- and DO-based PI-PD control schemes, while Figure 16 displays the frequency deviation responses. For the area-1 LFC, the LPBO-based PI-PD provided the quickest settling time of 5.21 s. For the area-2 and area-3 LFCs, all other proposed schemes had slower settling times than the DO-based PI-PD, which offered 7.59 s and 7.54 s, respectively. This means that the DO-based PI-PD controller provided, relatively, a 21%, 23% and 2% better settling time response compared with the AOA-, LPBO- and MPSO-based PI-PD controllers in area-2. Similarly, the DO-based PI-PD controller produced, relatively, a 20%, 10% and 4% better settling time response compared with the AOA-, LPBO- and MPSO-based PI-PD controllers in area-3. It is very clear that the % overshoot and undershoot are almost negligible in all areas with the proposed control schemes. Overall, it can be seen that the DO-based PI-PD outperforms other schemes in terms of settling time and % overshoot and undershoot responses. Moreover, with each control scheme applied to a given system, the steady-state error is zero.

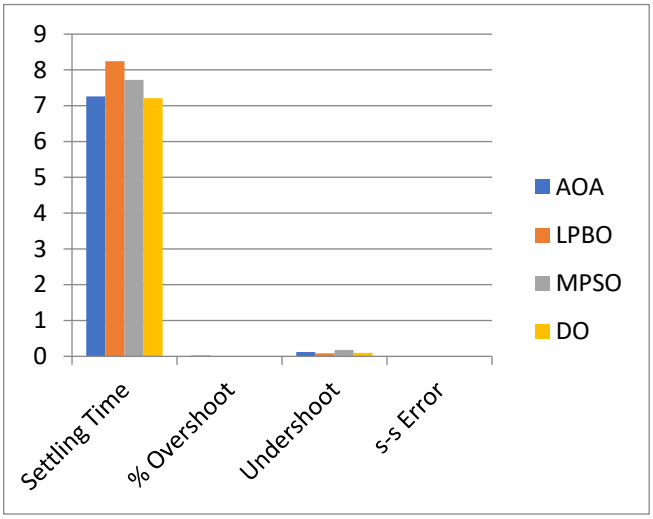

(**a**)

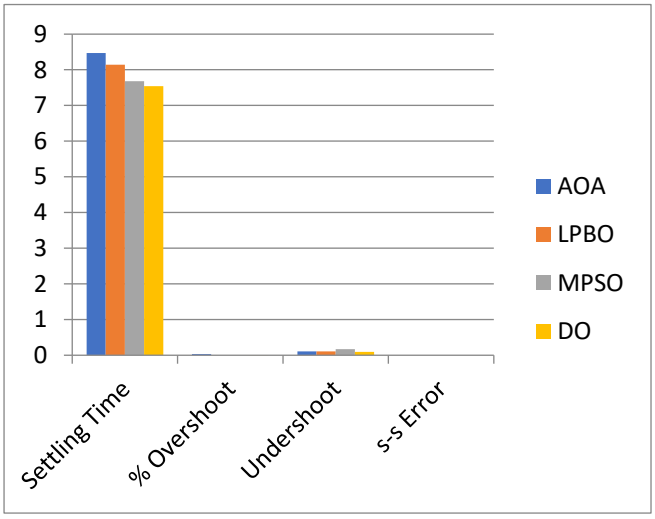

(**b**)

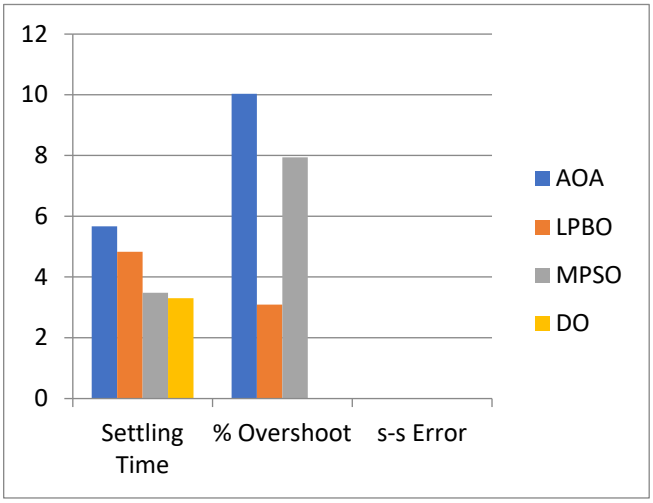

(**c**)

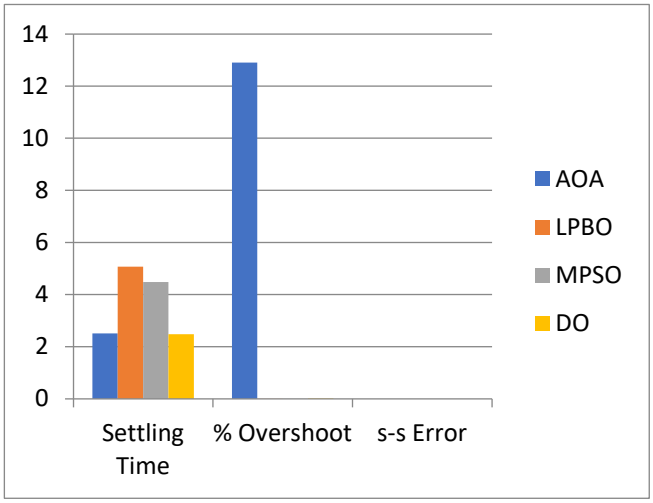

(**d**)

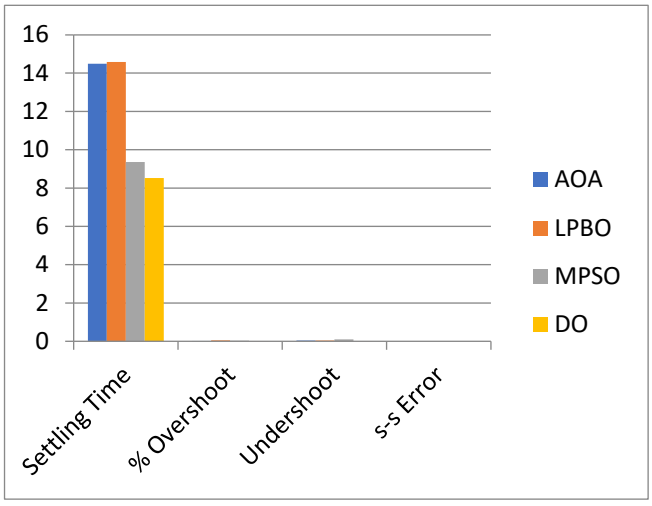

(**e**)

Figure 14. Graphical comparison in a two-area multi-source realistic IPS with nonlinearities. (**a**) Δf_1; (**b**) Δf_2; (**c**) V_{t1}; (**d**) V_{t2}; (**e**) $P_{tie\text{-}line}$.

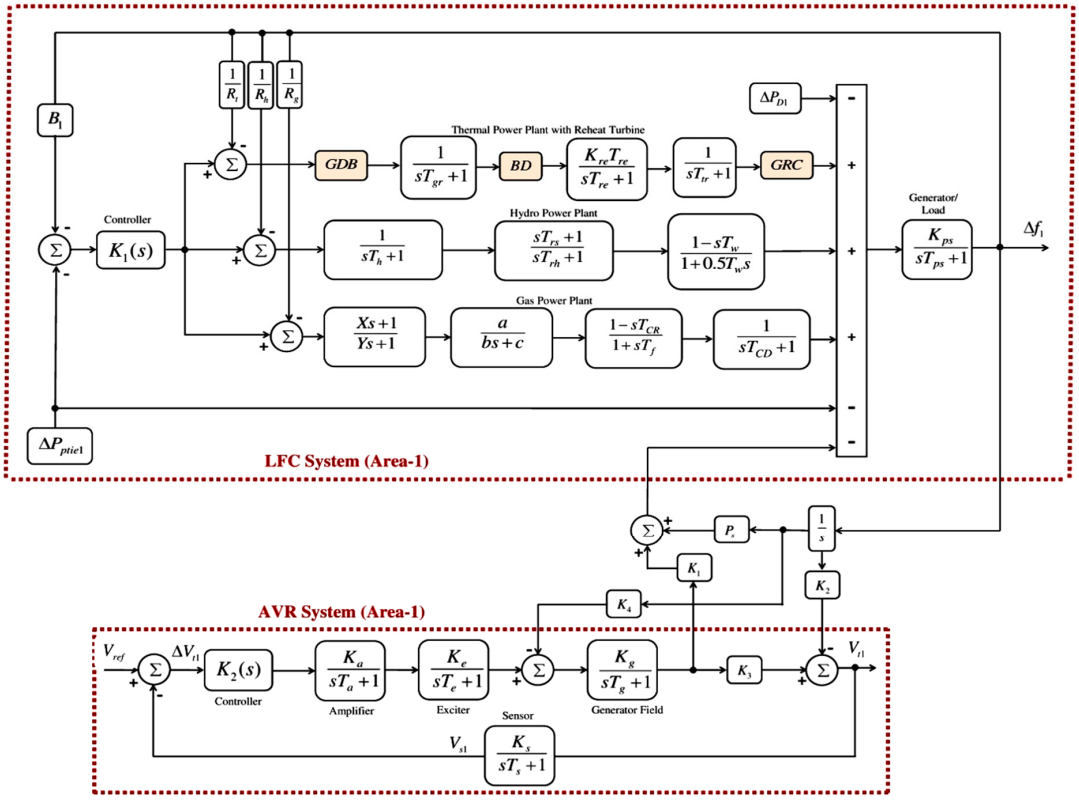

(**a**)

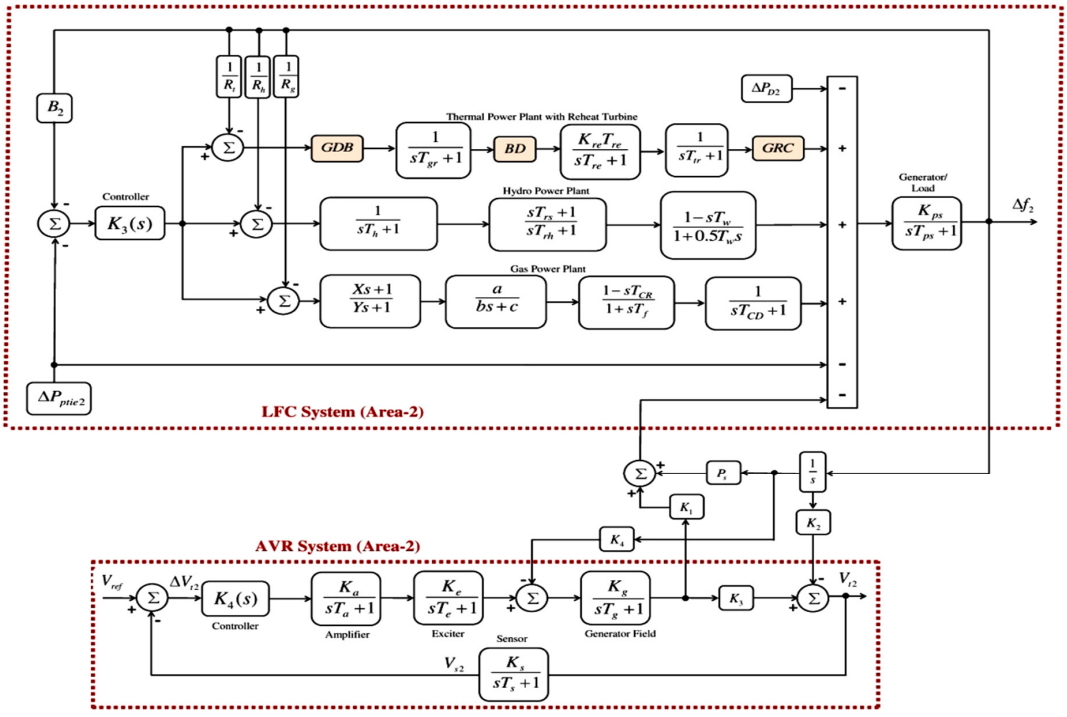

(**b**)

Figure 15. *Cont.*

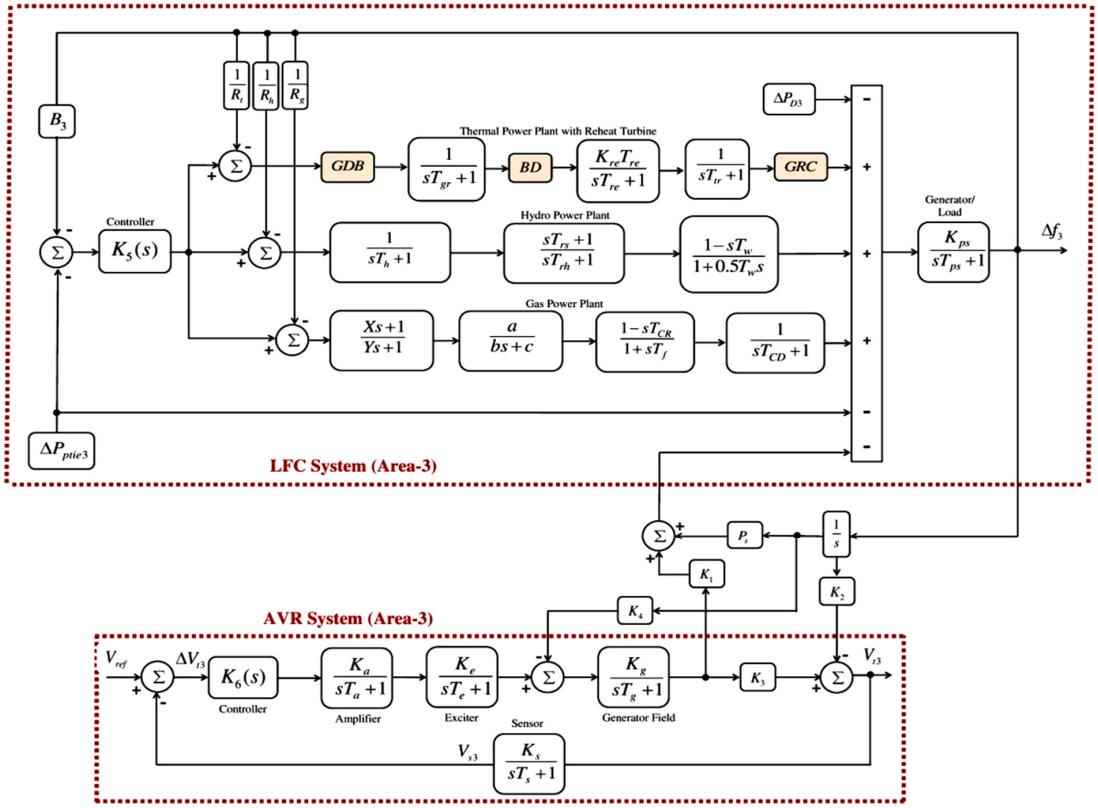

(**c**)

Figure 15. Three-area IPS with combined LFC-AVR. (**a**) Area-1; (**b**) Area-2; (**c**) Area-3.

Table 12. Optimal values of controller parameters in a three-area multi-source IPS with nonlinearities.

Area	Parameters of Controllers	AOA-Based PI-PD	LPBO-Based PI-PD	MPSO-Based PI-PD	DO-Based PI-PD
Area-1	K_{p1}	1.49	1.90	1.36	1.61
	K_{i1}	1.56	0.15	0.42	1.44
	K_{p2}	1.44	0	0.62	0.32
	K_{d1}	1.93	0.74	0.43	1.52
	K_{p3}	1.83	1.68	1.16	0.99
	K_{i2}	1.63	0.95	1.00	1.60
	K_{p4}	1.57	0.32	0.92	1.10
	K_{d2}	1.61	0.26	0.27	0.40
Area-2	K_{p5}	1.78	0.66	1.15	1.66
	K_{i3}	1.76	0.96	1.73	1.82
	K_{p6}	1.78	1.065	0.26	1.69
	K_{d3}	1.80	0.64	1.04	0.72
	K_{p7}	1.79	0.85	1.05	0.13
	K_{i4}	1.68	1.13	1.80	1.68
	K_{p8}	1.36	0.96	1.40	1.93
	K_{d4}	1.15	0.88	1.12	0.35
Area-3	K_{p9}	1.73	0.12	1.11	0.45
	K_{i5}	1.70	1.13	1.73	1.19
	K_{p10}	1.95	1.18	0.23	2
	K_{d5}	1.65	1.68	0.36	1.78
	K_{p11}	1.53	1.77	0.75	1.34
	K_{i6}	1.71	0.80	0.29	1.68
	K_{p12}	1.71	0.37	0.09	1.13
	K_{d6}	1.56	1.42	0.21	1.05
	ITSE	0.90	0.81	0.90	0.89

Table 13. Numerical results of LFC in a three-area multi-source IPS with nonlinearities.

Control Scheme	Area-1				Area-2				Area-3			
	Settling Time	% Overshoot	Undershoot	s-s Error	Settling Time	% Overshoot	Undershoot	s-s Error	Settling Time	% Overshoot	Undershoot	s-s Error
AOA-based PI-PD	9.48	0	−0.067	0	9.62	0	0.0027	0	9.41	0	−0.0068	0
LPBO-based PI-PD	5.21	0.0049	−0.19	0	9.89	0.0030	0.10	0	8.37	0.0057	−0.099	0
MPSO-based PI-PD	7.74	0.0032	−0.17	0	7.73	0.021	0.15	0	7.84	0.0041	−0.17	0
DO-based PI-PD	7.21	0	−0.10	0	7.59	0.00017	0.086	0	7.54	0	−0.075	0

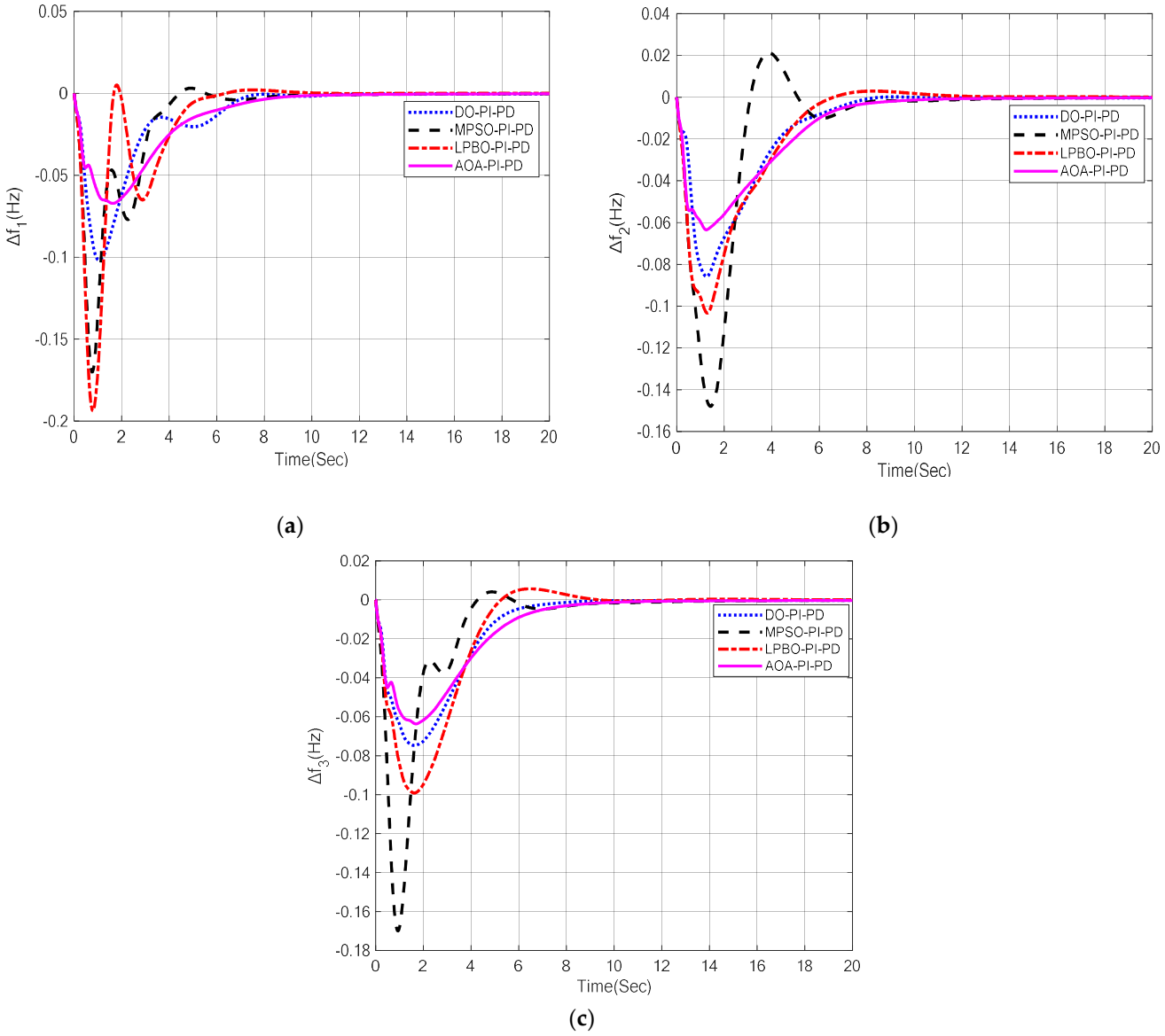

Figure 16. LFC responses in a three-area multi-source IPS with nonlinearities. (**a**) Δf_1; (**b**) Δf_2; (**c**) Δf_3.

Table 14 presents the numerical results of the terminal voltages in a three-area, three sources/area IPS and nonlinearities utilizing the DO-, AOA-, LPBO- and MPSO-based PI-PD control schemes, while Figure 17 displays the terminal voltage responses. In area-1, area-2 and area-3, respectively, the DO-based PI-PD achieved faster settling times of 3.27 s, 2.02 s and 2.23 s than other suggested techniques. This means the DO-based PI-PD controller provided, relatively, a 20%, 15% and 46% better settling time response compared with the AOA-, LPBO- and MPSO-based PI-PD controllers in the area-1 AVR, respectively. Moreover, the DO-based PI-PD controller produced, relatively, a 47.3%, 28% and 47.4% better settling

time response compared with the AOA-, LPBO- and MPSO-based PI-PD controllers in the area-2 AVR, respectively. Finally, the DO-based PI-PD controller yielded, relatively, a 41%, 61% and 68% better settling time response compared with the AOA-, MPSO- and LPBO-based PI-PD controllers in the area-3 AVR, respectively. As can be observed, the overshoot and undershoot are once more quite small in all areas of each control scheme. With each control scheme, the steady-state error is once again zero.

Table 14. Numerical results of AVR in a three-area multi-source IPS with nonlinearities.

Control Scheme	Area-1			Area-2			Area-3		
	Settling Time	% Overshoot	s-s Error	Settling Time	% Overshoot	s-s Error	Settling Time	% Overshoot	s-s Error
AOA-based PI-PD	4.09	0.013	0	3.83	0.0056	0	3.78	0.098	0
LPBO-based PI-PD	3.85	17.39	0	2.80	1.67	0	7.04	6.09	0
MPSO-based PI-PD	6.10	0	0	3.84	2.24	0	5.69	0	0
DO-based PI-PD	3.27	0.034	0	2.02	0.0009	0	2.23	1.65	0

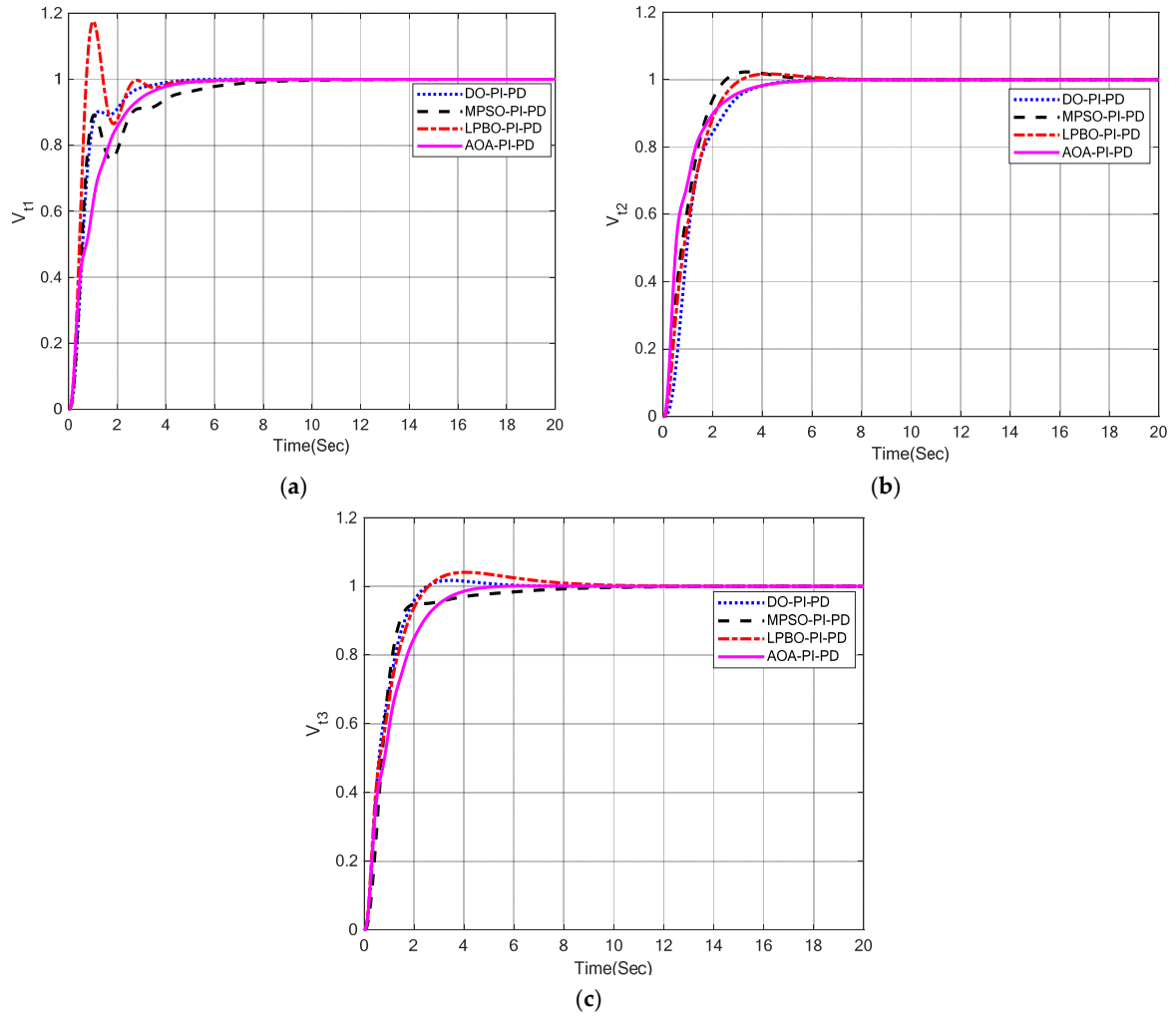

Figure 17. AVR response in a three-area multi-source IPS with nonlinearities. (**a**) V_{t1}; (**b**) V_{t2}; (**c**) V_{t3}.

Figure 18 shows the tie-line power deviation curves, and Table 15 presents the numerical results of tie-line power deviation in a three-area, three sources/area IPS with nonlinearities using DO-, AOA-, LPBO- and MPSO-based PI-PD control techniques. The DO-based PI-PD provided the quickest settling times of 10.79 s and 10.35 s in area-1 and area-3, respectively. In area-2, the MPSO-based PI-PD provided a settling time of 11.13 s, which is a little bit lower than the settling time of the DO-based PI-PD controller, which was 11.31 s. This means the DO-based PI-PD controller yielded, relatively, a 13%, 11% and 20% better settling time response compared with the AOA-, LPBO- and MPSO-based PI-PD controllers in area-1. Further, the DO-based PI-PD controller produced, relatively, a 2% and 7% better settling time response compared with the AOA- and LPBO-based PI-PD controllers in area-2. Finally, the DO-based PI-PD controller provided, relatively, a 12%, 24% and 13% better settling time response compared with the AOA-, LPBO- and MPSO-based PI-PD controllers in area-3. Overshoots were once again minimal in each control scheme in all areas. The performance metrics of the DO-, AOA-, LPBO- and MPSO-based PI-PD control techniques in a three-area multi-source IPS with nonlinearities are graphically compared in Figure 19. It is evident that the tie-line power deviation, terminal voltage and frequency responses of the DO-based PI-PD controller are significantly better than those of the other control methods.

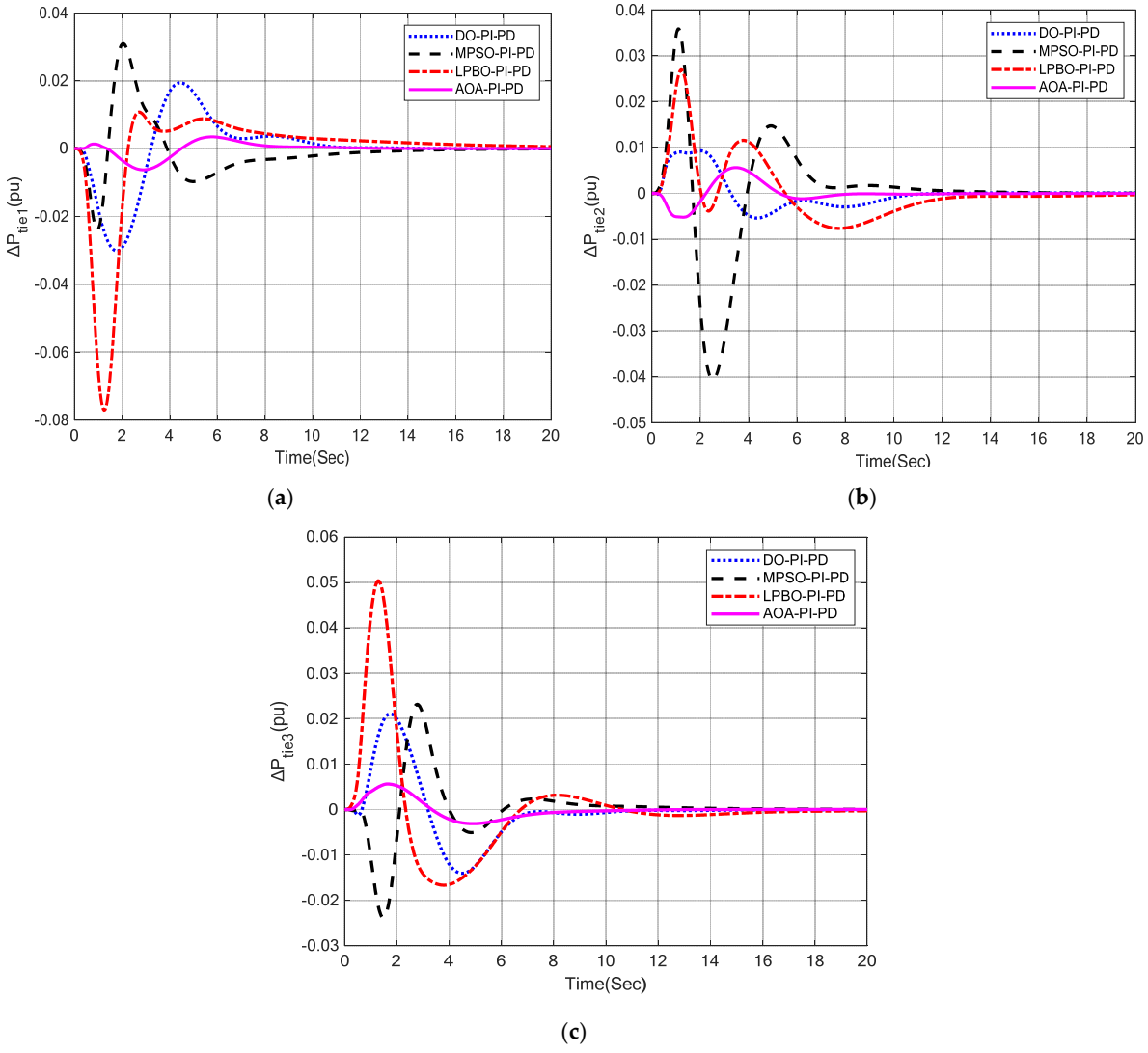

Figure 18. Tie-line power deviation responses in a three-area multi-source IPS with nonlinearities. (**a**) ΔP_{tie1}; (**b**) ΔP_{tie2}; (**c**) ΔP_{tie3}.

Table 15. Numerical results of tie-line power deviation in a three-area multi-source IPS with nonlinearities.

Control Scheme	Area-1				Area-2				Area-3			
	Settling Time	% Overshoot	Undershoot	s-s Error	Settling Time	% Overshoot	Undershoot	s-s Error	Settling Time	% Overshoot	Undershoot	s-s Error
AOA-based PI-PD	12.42	0.0035	−0.006	0	11.51	0.0056	−0.0052	0	11.71	0.0056	−0.0031	0
LPBO-based PI-PD	12.19	0.011	−0.077	0	12.21	0.027	−0.0076	0	13.64	0.050	−0.017	0
MPSO-based PI-PD	13.50	0.031	−0.024	0	11.13	0.036	−0.041	0	11.83	0.0232	−0.024	0
DO-based PI-PD	10.79	0.019	−0.030	0	11.31	0.0093	−0.0054	0	10.35	0.0211	−0.014	0

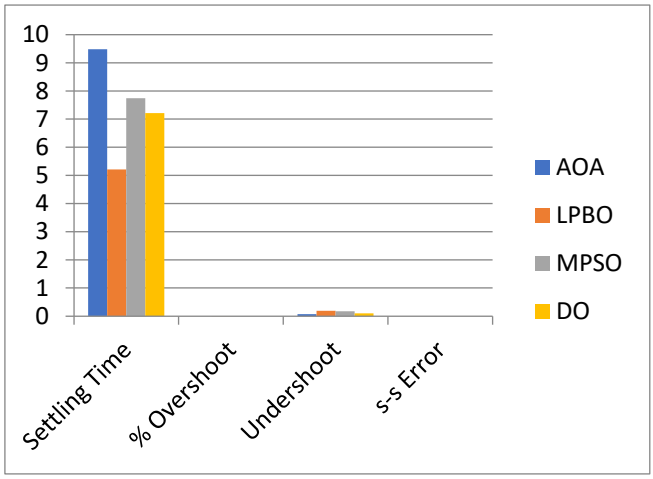

(**a**)

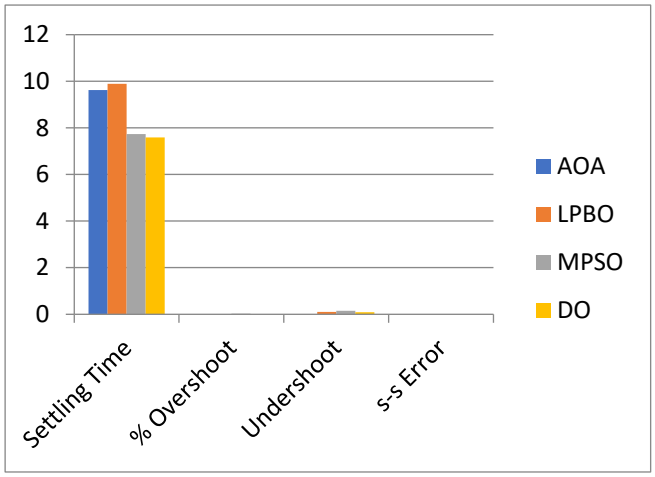

(**b**)

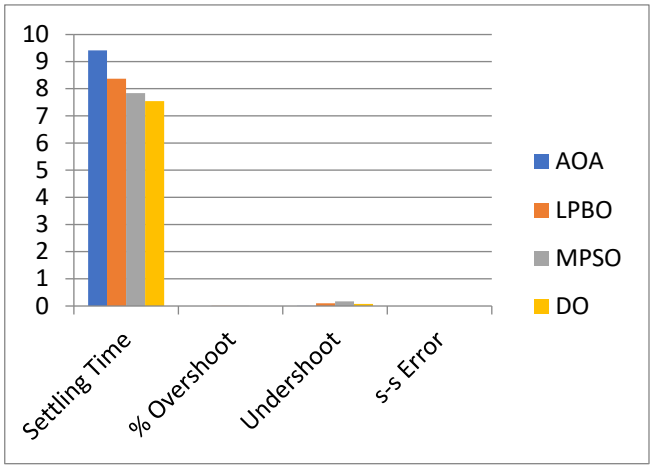

(**c**)

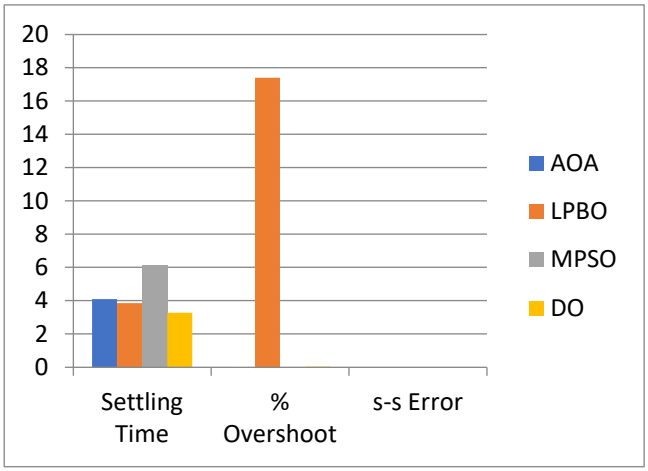

(**d**)

Figure 19. *Cont.*

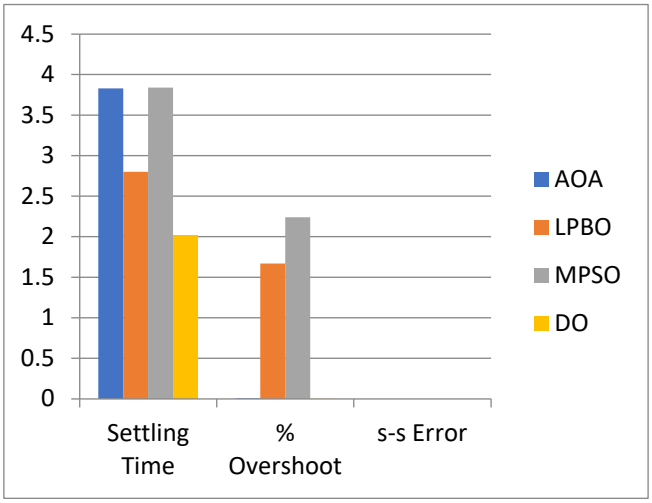

(**e**)

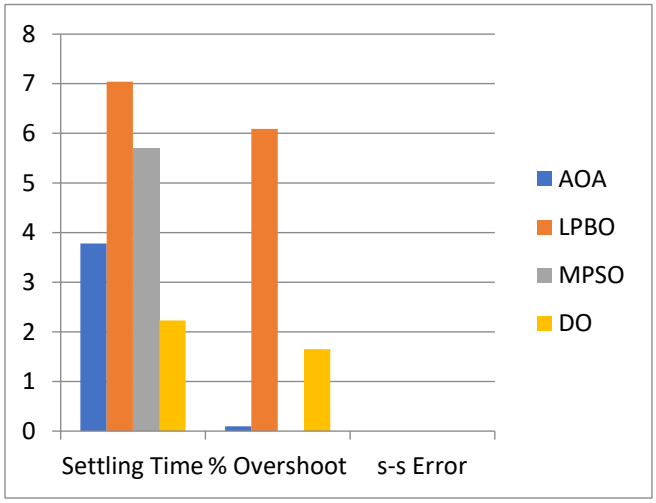

(**f**)

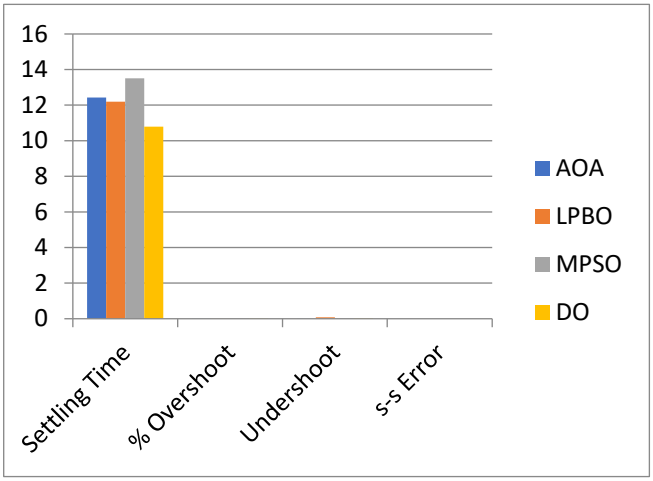

(**g**)

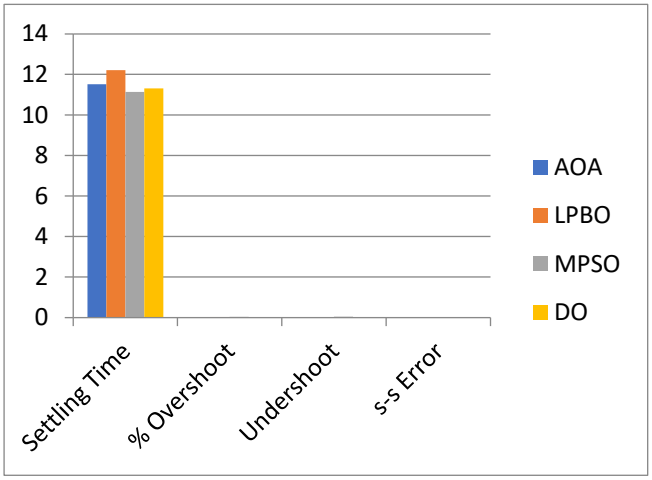

(**h**)

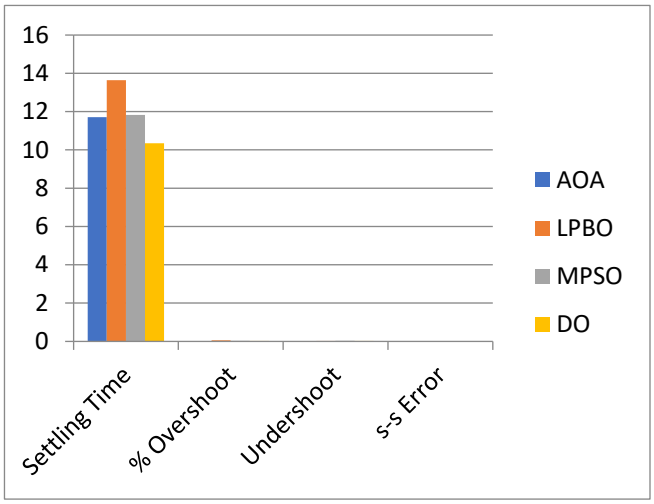

(**i**)

Figure 19. Graphical comparison in a three-area multi-source IPS with nonlinearities. (**a**) Δf_1; (**b**) Δf_2; (**c**) Δf_3; (**d**) V_{t1}; (**e**) V_{t2}; (**f**) V_{t3}; (**g**) ΔP_{tie1}; (**h**) ΔP_{tie2}; (**i**) ΔP_{tie3}.

6. Conclusions and Future Work

In this work, the performance of a multi-area, multi-source IPS with combined AVR-LFC loops was analyzed. Using DO-, AOA-, LPBO- and MPSO-based PI-PD control schemes, the multi-area, multi-source IPS was studied in detail. For a two-area multi-source IPS with 10% SLP in area-1, DO-,AOA-, LPBO- and MPSO-based PI-PDs yielded 53%, 47%, 39% and 52% quicker settling time responses in the area-1 LFC, whereas they had 32%, 26%, 12% and 32% improved settling times in the area-2 LFC, respectively, compared with the HAEFA Fuzzy PID controller [3], as demonstrated in Table 5. Similarly, the DO-based PI-PD came up with 40% and 31% better settling times than the HAEFA Fuzzy PID in the area-1 and area-2 AVRs, respectively. Moreover, the DO-, AOA-, LPBO- and MPSO-based PI-PDs provided 86%, 99.9%, 10% and 96% better % overshoot responses in the area-1 AVR and 86%, 99.7%, 99.8% and 99.9% better % overshoot responses in area-2 AVR, respectively, compared with the HAEFA Fuzzy PID controller, as presented in Table 6. In comparison with the HAEFA Fuzzy PID controller, it can be seen that the DO-, AOA-, LPBO- and MPSO-based PI-PDs provided 43%, 18%, 75% and 12% rapid tie-line settling time responses, respectively, as depicted in Table 7. For two- and three-area realistic IPSs with nonlinearities and different SLPs, the DO-based PI-PD yielded relatively better LFC settling time responses in both areas compared with the AOA-, LPBO- and MPSO-based PI-PD control schemes, as demonstrated in Tables 9 and 13, respectively. Similarly, the DO-based PI-PD produced relatively better AVR settling times and % overshoot responses in both areas compared with the AOA-, LPBO- and MPSO-based PI-PD control schemes, as illustrated in Tables 10 and 14, respectively. Finally, the DO-based PI-PD yielded relatively better tie-line power deviation settling time responses compared with the AOA-, LPBO- and MPSO-based PI-PD control schemes in both areas, as presented in Tables 11 and 15, respectively. The results show that the use of the proposed DO-based PI-PD control scheme is highly recommended for multi-area multi-source IPSs with nonlinearities. Considering the importance of the work performed so far, in the future, we would like to analyze multi-area, multi-source IPSs with neuro-fuzzy, fractional order and hybrid ANN controllers. In addition, relatively recently developed nature-inspired computational methods such as sea-horse optimization, artificial rabbits optimization, etc., can be explored to determine the best controller parameters for this type of application.

Author Contributions: Conceptualization, T.A. (Tayyab Ali) and S.A.M.; methodology, T.A. (Tayyab Ali) and S.A.M.; validation, S.A.M., A.D. and S.A.; formal analysis, S.A.M., A.D. and S.A.; investigation, T.A. (Tayyab Ali) and S.A.M.; resources, A.D. and S.A.; data curation, T.A. (Tayyab Ali), S.A.M. and A.D.; writing—original draft preparation, T.A. (Tayyab Ali) and S.A.M.; writing—review and editing, T.A. (Tayyab Ali), S.A.M., A.D., S.A. and T.A. (Tamim Alkhalifah); supervision, S.A.M., A.D. and S.A.; funding acquisition, T.A. (Tamim Alkhalifah); All authors have read and agreed to the published version of the manuscript.

Funding: The researchers would like to thank the Deanship of Scientific Research, Qassim University, for funding the publication of this project.

Institutional Review Board Statement: Not applicable.

Informed Consent Statement: Not applicable.

Data Availability Statement: Not applicable.

Conflicts of Interest: The authors declare no conflict of interest.

Appendix A. Power System Parameters and Their Values

Parameter	Value	Parameter	Value
B_1, B_2, B_3	0.045	H	5
f	60	$K_{ps} = 1/D$	68.97
R_t	2.4	$T_{ps} = 2 * H/f * D$	11.49
R_h	2.4	K_1	0.2
R_g	2.4	K_2	0.1
T_{gr}	0.08	K_3	0.5
T_{re}	10	K_4	1.4
K_{re}	0.3	P_s	1.5
T_{tr}	0.3	K_a	10
T_h	0.3	T_a	0.1
T_{rs}	5	K_e	1
T_{rh}	28.75	T_e	0.4
T_w	0.025	K_g	0.8
X	0.6	T_g	1.4
Y	1	K_s	1
a	1	T_s	0.05
b	0.05	T_{12}	0.545
c	1	T_{13}	0.545
T_{cr}	0.01	T_{21}	0.545
T_f	0.23	T_{22}	0.545
T_{cd}	0.2	T_{31}	0.545
D	0.0145	T_{32}	0.545

References

1. Dekaraja, B.; Saikia, L.C. Combined Voltage and Frequency Control of Multiarea Multisource System Using CPDN-PIDN Controller. *IETE J. Res.* **2021**, 1–16. [CrossRef]
2. Ghosh, A.; Ray, A.K.; Nurujjaman, M.; Jamshidi, M. Voltage and frequency control in conventional and PV integrated power systems by a particle swarm optimized Ziegler-Nichols based PID controller. *SN Appl. Sci.* **2021**, *3*, 1–13. [CrossRef]
3. Kalyan, C.N.S.; Goud, B.S.; Reddy, C.R.; Bajaj, M.; Sharma, N.K.; Alhelou, H.H.; Siano, P.; Kamel, S. Comparative Performance Assessment of Different Energy Storage Devices in Combined LFC and AVR Analysis of Multi-Area Power System. *Energies* **2022**, *15*, 629. [CrossRef]
4. Ali, T.; Malik, S.A.; Hameed, I.A.; Daraz, A.; Mujlid, H.; Azar, A.T. Load Frequency Control and Automatic Voltage Regulation in a Multi-Area Interconnected Power System Using Nature-Inspired Computation-Based Control Methodology. *Sustainability* **2022**, *14*, 12162. [CrossRef]
5. Fayek, H.H.; Rusu, E. Novel Combined Load Frequency Control and Automatic Voltage Regulation of a 100% Sustainable Energy Interconnected Microgrids. *Sustainability* **2022**, *14*, 9428. [CrossRef]
6. Dekaraja, B.; Saikia, L.C.; Ramoji, S.K.; Behera, M.K.; Bhagat, S.K. Performance Analysis of Diverse Energy Storage on Combined ALFC and AVR Control of Multiarea Multiunit System with AC/HVDC interconnection. *IFAC-Pap. OnLine* **2022**, *55*, 479–485. [CrossRef]
7. Dekaraja, B.; Saikia, L.C.; Ramoji, S.K. Combined ALFC-AVR Control of Diverse Energy Source Based Interconnected Power System using Cascade Controller. In Proceedings of the 2022 International Conference on Intelligent Controller and Computing for Smart Power (ICICCSP), Hyderabad, India, 21–23 July 2022; pp. 1–6. [CrossRef]
8. Dekaraja, B.; Saikia, L.C.; Ramoji, S.K.; Behera, M.K.; Bhagat, S.K. Impact of RFB and HVDC link on Combined ALFC-AVR Studies of a GTPP Integrated Hydro-Thermal Systems Using a Cascade Fuzzy PD-TID Controller. In Proceedings of the 4th International Conference on Energy, Power and Environment (ICEPE), Shillong, India, 29 April–1 May 2022; pp. 3–8. [CrossRef]
9. Ramoji, S.K.; Saikia, L.C.; Dekaraja, B.; Behera, M.K.; Bhagat, S.K. Performance Comparison of Various Tilt Controllers in Coalesced Voltage and Frequency Regulation of Multi-Area Multi-Unit Power System. In Proceedings of the IEEE Delhi Section Conference (DELCON), New Delhi, India, 11–13 February 2022. [CrossRef]
10. Safiullah, S.; Rahman, A.; Aftab, M.A.; Hussain, S.M.S. Performance study of ADRC and PID for concurrent Frequency-Voltage Control of Electric Vehicle Incorporated Hybrid Power System. In Proceedings of the PESGRE 2022—IEEE International Conference on Power Electronics, Smart Grid, and Renewable Energy (PESGRE), Trivandrum, India, 2–5 January 2022. [CrossRef]
11. Ramoji, S.K.; Saikia, L.C. Optimal Coordinated Frequency and Voltage Control of CCGT-Thermal Plants with TIDF Controller. *IETE J. Res.* **2021**, 1–18. [CrossRef]
12. Oladipo, S.; Sun, Y.; Wang, Z. An effective hFPAPFA for a PIDA-based hybrid loop of Load Frequency and terminal voltage regulation system. In Proceedings of the 2021 IEEE PES/IAS PowerAfrica, PowerAfrica 2021, Nairobi, Kenya, 23–27 August 2021. [CrossRef]
13. Anusha, P.; Patra, S.; Roy, A.; Saha, D. Combined Frequency and Voltage Control of a Deregulated Hydro-Thermal Power System employing FA based Industrial Controller. In Proceedings of the2021 International Conference on Computational Performance Evaluation (ComPE), Shillong, India, 1–3 December 2021; pp. 848–853. [CrossRef]
14. Kalyan, C.N.S. UPFC and SMES based Coordinated Control Strategy for Simultaneous Frequency and Voltage Stability of an Interconnected Power System. In Proceedings of the 1st International Conference on Power Electronics and Energy (ICPEE), Bhubaneswar, India, 2–3 January 2021. [CrossRef]
15. Nahas, N.; Abouheaf, M.; Darghouth, M.N.; Sharaf, A. A multi-objective AVR-LFC optimization scheme for multi-area power systems. *Electr. Power Syst. Res.* **2021**, *200*, 107467. [CrossRef]

16. Prakash, A.; Parida, S.K. Combined frequency and voltage stabilization of thermal-thermal system with UPFC and RFB. In Proceedings of the PIICON 2020—9th IEEE Power India International Conference (PIICON), Sonepat, India, 28 February–1 March 2020. [CrossRef]
17. Kalyan, C.H.N.S.; Rao, G.S. Combined frequency and voltage stabilisation of multi-area multisource system by DE-AEFA optimised PID controller with coordinated performance of IPFC and RFBs. *Int. J. Ambient. Energy* **2020**, 1–20. [CrossRef]
18. Kalyan, C.H.N.S.; Rao, G.S. Frequency and voltage stabilisation in combined load frequency control and automatic voltage regulation of multiarea system with hybrid generation utilities by AC/DC links. *Int. J. Sustain. Energy* **2020**, *39*, 1009–1029. [CrossRef]
19. Morsali, J.; Esmaeili, Z. Proposing a new hybrid model for LFC and AVR loops to improve effectively frequency stability using coordinative CPSS. In Proceedings of the 28th Iranian Conference on Electrical Engineering (ICEE), Tabriz, Iran, 4–6 August 2020. [CrossRef]
20. Nahas, N.; Abouheaf, M.; Sharaf, A.; Gueaieb, W. A Self-Adjusting Adaptive AVR-LFC Scheme for Synchronous Generators. *IEEE Trans. Power Syst.* **2019**, *34*, 5073–5075. [CrossRef]
21. Sahani, A.K.; Raj, U.; Shankar, R.; Mandal, R.K. Firefly optimization based control strategies for combined load frequency control and automatic voltage regulation for two-area interconnected power system. *Int. J. Electr. Eng. Inform.* **2019**, *11*, 747–758. [CrossRef]
22. Lal, D.K.; Barisal, A.K. Combined load frequency and terminal voltage control of power systems using moth flame optimization algorithm. *J. Electr. Syst. Inf. Technol.* **2019**, *6*, 1–24. [CrossRef]
23. Rajbongshi, R.; Saikia, L.C. Coordinated performance of interline power flow controller and superconducting magnetic energy storage in combined ALFC and AVR system under deregulated environment. *J. Renew. Sustain. Energy* **2018**, *10*, 044102. [CrossRef]
24. Sharma, D.; Kushwaha, V.; Pandey, K.; Rani, N. Intelligent avr control of a single thermal area combined with lfc loop. *Adv. Intell. Syst. Comput.* **2018**, *624*, 779–789. [CrossRef]
25. Gupta, M.; Srivastava, S.; Gupta, J.R.P. A Novel Controller for Model with Combined LFC and AVR Loops of Single Area Power System. *J. Inst. Eng. Ser. B* **2014**, *97*, 21–29. [CrossRef]
26. Kumar, V. Model Predictive Controller-Based Voltage and Frequency Regulation in Renewable Energy Integrated Power System Coordinated with Virtual Inertia and Redox Flow Battery. *Iran. J. Sci. Technol. Trans. Electr. Eng.* **2022**, 0123456789. [CrossRef]
27. Sijakovic, N.; Terzic, A.; Fotis, G.; Mentis, I.; Zafeiropoulou, M.; Maris, T.I.; Zoulias, E.; Elias, C.; Ristic, V.; Vita, V. Active System Management Approach for Flexibility Services to the Greek Transmission and Distribution System. *Energies* **2022**, *15*, 6134. [CrossRef]
28. Adewumi, O.B.; Fotis, G.; Vita, V.; Nankoo, D.; Ekonomou, L. The Impact of Distributed Energy Storage on Distribution and Transmission Networks' Power Quality. *Appl. Sci.* **2022**, *12*, 6466. [CrossRef]
29. Daraz, A.; Malik, S.A.; Waseem, A.; Azar, A.T.; Haq, I.U.; Ullah, Z.; Aslam, S. Automatic generation control of multi-source interconnected power system using FOI-TD controller. *Energies* **2021**, *14*, 5867. [CrossRef]
30. Daraz, A.; Malik, S.A.; Mokhlis, H.; Haq, I.U.; Laghari, G.F.; Mansor, N.N. Fitness Dependent Optimizer-Based Automatic Generation Control of Multi-Source Interconnected Power System with Non-Linearities. *IEEE Access* **2020**, *8*, 100989–101003. [CrossRef]
31. Daraz, A.; Malik, S.A.; Mokhlis, H.; Haq, I.U.; Zafar, F.; Mansor, N.N. Improved-Fitness Dependent Optimizer Based FOI-PD Controller for Automatic Generation Control of Multi-Source Interconnected Power System in Deregulated Environment. *IEEE Access* **2020**, *8*, 197757. [CrossRef]
32. Daraz, A.; Malik, S.A.; Azar, A.T.; Aslam, S.; Alkhalifah, T.; Alturise, F. Optimized Fractional Order Integral-Tilt Derivative Controller for Frequency Regulation of Interconnected Diverse Renewable Energy Resources. *IEEE Access* **2022**, *10*, 43514–43527. [CrossRef]
33. Daraz, A.; Malik, S.A.; Haq, I.U.; Khan, K.B.; Laghari, G.F.; Zafar, F. Modified PID controller for automatic generation control of multi-source interconnected power system using fitness dependent optimizer algorithm. *PLoS ONE* **2020**, *15*, e0242428. [CrossRef]
34. Wang, L.; Cao, Q.; Zhang, Z.; Mirjalili, S.; Zhao, W. Artificial rabbits optimization: A new bio-inspired meta-heuristic algorithm for solving engineering optimization problems. *Eng. Appl. Artif. Intell.* **2022**, *114*, 105082. [CrossRef]
35. Zhao, S.; Zhang, T.; Ma, S.; Chen, M. Dandelion Optimizer: A nature-inspired metaheuristic algorithm for engineering applications. *Eng. Appl. Artif. Intell.* **2022**, *114*, 105075. [CrossRef]
36. Zhao, S.; Zhang, T.; Ma, S.; Wang, M. Sea-horse optimizer: A novel nature-inspired meta-heuristic for global optimization problems. *Appl. Intell.* **2022**. [CrossRef]
37. Hashim, F.A.; Hussain, K.; Houssein, E.H.; Mabrouk, M.S.; Al-Atabany, W. Archimedes optimization algorithm: A new metaheuristic algorithm for solving optimization problems. *Appl. Intell.* **2020**, *51*, 1531–1551. [CrossRef]
38. MQais, H.; Hasanien, H.M.; Alghuwainem, S. Transient search optimization: A new meta-heuristic optimization algorithm. *Appl. Intell.* **2020**, *50*, 3926–3941. [CrossRef]
39. Rahman, C.M.; Rashid, T.A. A new evolutionary algorithm: Learner performance based behavior algorithm. *Egypt. Inform. J.* **2021**, *22*, 213–223. [CrossRef]
40. Guha, D.; Roy, P.K.; Banerjee, S. Application of backtracking search algorithm in load frequency control of multi-area interconnected power system. *Ain Shams Eng. J.* **2018**, *9*, 257–276. [CrossRef]

41. Guha, D.; Roy, P.K.; Banerjee, S. Symbiotic organism search algorithm applied to load frequency control of multi-area power system. *Energy Syst.* **2018**, *9*, 439–468. [CrossRef]
42. Tripathy, S.C.; Balasubramanian, R.; Nair, P.S.C. Effect of Superconducting Magnetic Energy Storage on Automatic Generation Control Considering Governor Deadband and Boiler Dynamics. *IEEE Trans. Power Syst.* **1992**, *7*, 1266–1273. [CrossRef]
43. Zou, H.; Li, H. Tuning of PI-PD controller using extended non-minimal state space model predictive control for the stabilized gasoline vapor pressure in a stabilized tower. *Chemom. Intell. Lab. Syst.* **2015**, *142*, 1–8. [CrossRef]
44. Raja, G.L.; Ali, A. New PI-PD Controller Design Strategy for Industrial Unstable and Integrating Processes with Dead Time and Inverse Response. *J. Control Autom. Electr. Syst.* **2021**, *32*, 266–280. [CrossRef]
45. Kaya, I. Optimal PI-PD Controller Design for Pure Integrating Processes with Time Delay. *J. Control Autom. Electr. Syst.* **2021**, *32*, 563–572. [CrossRef]
46. Irshad, M.; Ali, A. Robust PI-PD controller design for integrating and unstable processes. *IFAC-Pap. OnLine* **2020**, *53*, 135–140. [CrossRef]
47. Peram, M.; Mishra, S.; Vemulapaty, M.; Verma, B.; Padhy, P.K. Optimal PI-PD and I-PD Controller Design Using Cuckoo Search Algorithm. In Proceedings of the 5th Conference on Signal Processing and Integrated Networks (SPIN), Noida, India, 2–3 February 2018; pp. 643–646. [CrossRef]
48. Ali, T.; Malik, S.A.; Adeel, M.; Amir, M. Set point tracking of Ball and Beam System Using Genetic Algorithm based PI-PD Controller. *NUST J. Eng. Sci.* **2018**, *11*, 12–16. [CrossRef]
49. Zheng, M.; Huang, T.; Zhang, G. A New Design Method for PI-PD Control of Unstable Fractional-Order System with Time Delay. *Complexity* **2019**, *2019*, 3253497. [CrossRef]
50. Ali, T.; Adeel, M.; Malik, S.A.; Amir, M. Stability Control of Ball and Beam System Using Heuristic Computation Based PI-D and PI-PD Controller. *Tech. J.* **2019**, *24*, 21–29.